5-2011

Use of a Spine Robot Employing a Real Time Force Control Algorithm to Develop, Simulate, and Compare Spinal Biomechanical Testing Protocols: Eccentric Loading, Pure Moment, and a Novel Head Weight Protocol

Daniel Mark Wido
University of Tennessee Health Science Center

Use of a Spine Robot Employing a Real Time Force Control Algorithm to Develop, Simulate, and Compare Spinal Biomechanical Testing Protocols: Eccentric Loading, Pure Moment, and a Novel Head Weight Protocol

Abstract

In vitro testing provides a critical tool for understanding the biomechanics of the subaxial cervical spine. Previous common testing protocols used to evaluate the subaxial cervical spine include Pure Moment (PM), follower load, and eccentric lever arm (EL) loading methods. Although these methods are widely accepted, there is always a goal to try to better simulate physiologic loading conditions. While the follower load attempts to simulate compression due to muscle activation, no previous protocol has taken into account the constant vertical force vector applied to C2 produced by the weight of the human head. Furthermore, we are unaware of previous direct protocol to protocol comparisons using the same testing platform and test specimens. A novel protocol, the Head Weight Loading (HWL) protocol, was developed to maintain a constant vertical head weight vector of 65 N on the cranial specimen end throughout an entire range of motion. The objective of this study was to simulate and compare the EL protocol, PM protocol, and the newly developed HWL protocol on a single programmable robotic testing frame with a consistent specimen sample group.

Six fresh subaxial human cadaveric cervical spines (C2-T1) were screened using anteroposterior and lateral radiographs to ensure specimen quality. The EL, PM, and HWL protocols were simulated with global rotation through flexion and extension paths to a nondestructive 3 Nm end limit. Global spinal forces, moment, translational and rotational displacement data were recorded from the robot. Individual vertebral body rotations were measured using an optical non contact motion measurement system. Each motion segment unit's (MSU) percent contribution to overall motion was used to compare the protocols.

In flexion, the HWL protocol demonstrated significantly less motion at the C7-T1 MSU as compared to the EL and PM simulated protocols. A trend was noted for the HWL protocol to increase motion contributions in the cranial region (C2-C5) and reduce contributions at caudal levels (C5-T1). In extension an opposite trend was noted with motion contribution of the cranial levels, C2-C3 and C3-C4, significantly lower in the HWL protocol, whereas in the caudal, C6-C7 and C7-T1 levels, it was significantly higher.

The Spine Robot's ability to control end loads in real time enable it to execute a variety of biomechanical tests, making it unique in its ability to directly compare different protocols. The different end load conditions investigated produced significantly different MSU motion responses. The EL protocol has previously been reported to produce a more physiologic moment distribution compared to other standard protocols. However, due to fixturing constraints, it cannot produce loads at C2 that simulate head weight in vivo. The HWL protocol attempted to correct this and simulate an always present vertical force on the spine from the head. Studies incorporating the HWL protocol to study surgical alterations of the cervical spine are in progress, as well as use of the Spine Robot to develop new loading protocols.

Document Type

Thesis

Degree Name

Master of Science (MS)

Program

Biomedical Engineering

USE OF A SPINE ROBOT EMPLOYING A REAL TIME FORCE CONTROL ALGORITHM TO DEVELOP, SIMULATE, AND COMPARE SPINAL BIOMECHANICAL TESTING PROTOCOLS: ECCENTRIC LOADING, PURE MOMENT, AND A NOVEL HEAD WEIGHT PROTOCOL

A Thesis
Presented for
The Graduate Studies Council
The University of Tennessee
Health Science Center

In Partial Fulfillment
Of the Requirements for the Degree
Master of Science
In the Joint Graduate Program in Biomedical Engineering and Imaging
From The University of Tennessee
and
The University of Memphis

By
Daniel Mark Wido
May 2011

DEDICATION

In appreciation of my family
Mark, Judy, and Katherine Wido.

ACKNOWLEDGEMENTS

I would like to thank everyone who has given their time and advice in support of my educational career. Specifically, Dr. Brian Kelly, my research advisor, for giving me the opportunity to study at the UTHSC, as well as, for his instruction and mentorship. I would also like to thank Dr. Denis DiAngelo and Dr. Gladius Lewis for serving on my committee and providing valuable input on my research. I would like to recognize my colleagues, Braham Dhillon and Jessica Stubbs for their testing assistance. Special appreciation must be given to two undergraduate professors and mentors; Dr. Kevin Meade, for giving me my first opportunity to explore the world of biomechanics and Dr. Jai Prakash, for his support and guidance from high school onwards. Finally, I would like to thank my family, without their support and love this journey would have been much more difficult and less enjoyable.

ABSTRACT

In vitro testing provides a critical tool for understanding the biomechanics of the subaxial cervical spine. Previous common testing protocols used to evaluate the subaxial cervical spine include Pure Moment (PM), follower load, and eccentric lever arm (EL) loading methods. Although these methods are widely accepted, there is always a goal to try to better simulate physiologic loading conditions. While the follower load attempts to simulate compression due to muscle activation, no previous protocol has taken into account the constant vertical force vector applied to C2 produced by the weight of the human head. Furthermore, we are unaware of previous direct protocol to protocol comparisons using the same testing platform and test specimens. A novel protocol, the Head Weight Loading (HWL) protocol, was developed to maintain a constant vertical head weight vector of 65 N on the cranial specimen end throughout an entire range of motion. The objective of this study was to simulate and compare the EL protocol, PM protocol, and the newly developed HWL protocol on a single programmable robotic testing frame with a consistent specimen sample group.

Six fresh subaxial human cadaveric cervical spines (C2-T1) were screened using antero-posterior and lateral radiographs to ensure specimen quality. The EL, PM, and HWL protocols were simulated with global rotation through flexion and extension paths to a nondestructive 3 Nm end limit. Global spinal forces, moment, translational and rotational displacement data were recorded from the robot. Individual vertebral body rotations were measured using an optical non contact motion measurement system. Each motion segment unit's (MSU) percent contribution to overall motion was used to compare the protocols.

In flexion, the HWL protocol demonstrated significantly less motion at the C7-T1 MSU as compared to the EL and PM simulated protocols. A trend was noted for the HWL protocol to increase motion contributions in the cranial region (C2-C5) and reduce contributions at caudal levels (C5-T1). In extension an opposite trend was noted with motion contribution of the cranial levels, C2-C3 and C3-C4, significantly lower in the HWL protocol, whereas in the caudal, C6-C7 and C7-T1 levels, it was significantly higher.

The Spine Robot's ability to control end loads in real time enable it to execute a variety of biomechanical tests, making it unique in its ability to directly compare different protocols. The different end load conditions investigated produced significantly different MSU motion responses. The EL protocol has previously been reported to produce a more physiologic moment distribution compared to other standard protocols. However, due to fixturing constraints, it cannot produce loads at C2 that simulate head weight *in vivo*. The HWL protocol attempted to correct this and simulate an always present vertical force on the spine from the head. Studies incorporating the HWL protocol to study surgical alterations of the cervical spine are in progress, as well as use of the Spine Robot to develop new loading protocols.

TABLE OF CONTENTS

LIST OF FIGURES

LIST OF ABBREVIATIONS

Θ	Theta (degrees)
C(#)	Cervical Vertebral Body
EL	Eccentric Loading
Fx	Shear Force
Fz	Axial Force
HWL	Head Weight Loading
IVD	Intervertebral Disc
LED	Light Emitting Diode
MSU	Motion Segment Unit
N	Newtons
Nm	Newton-meters
PID	Intradiscal Pressure
PM	Pure Moment
ROM	Range of Motion
T(#)	Thoracic Vertebral Body
WCS	World Coordinate System

CHAPTER 1. INTRODUCTION

Neck and back pain are extremely common and costly afflictions. It is estimated 80% of the population will experience back pain at some point in their live (Valfours, 1985). In the United States, healthcare and workers compensation costs amount to over $50 billion per year (Siddharthan *et al*., 2005). The prevalence of back and neck pain has led to a large increase in the development of surgical procedures and novel instrumentation options for treatment. Correspondingly, an increased demand has been placed on biomechanical testing for evaluation of these new procedures and devices.

The pure moment protocol is a standard biomechanical testing protocol. It has been used to evaluate surgical techniques, fusion, and non-fusion devices in both the lumbar and cervical spine. The protocol is widely used due to its basic end loading configuration, in which a free spinal end is subjected to a bending moment in the plane of motion desired (Panjabi *et al*., 2007). Another common protocol is the Eccentric Loading protocol. Similarly, the protocol has been used in a wide variety of testing, but the end loading conditions incorporate a force component that causes a moment distribution along the spine (DiAngelo *et al*., 2003). Though both protocols are accepted they are not without limitation. The pure moment protocol omits compression and shear forces known to occur *in vivo* and may not simulate physiologic motions as measured *in vivo*. The EL protocol traditionally requires the spine to be mounted upside down thus creating a compressive force directed cranially, additionally, the shear and compression force magnitudes are created by fixture weight and may not be indicative of the actual *in vivo* loads. To improve on these limitations, the spinal biomechanics community is continually working toward creating in vitro scenarios that approximate *in vivo* conditions.

The objectives of this research were to, 1) use the Spine Robot to simulate and directly compare two gold standard biomechanical testing protocols, and 2) use the Spine Robot to develop a unique loading scenario that incorporates the influence of the vertical head weight force vector and compare the new protocol to accepted testing standards. It is hoped that the effect of end loading conditions on the motion response of the subaxial cervical spine will be better understood following this study. Chapters 3 and 4 contain manuscripts detailing the work, which are intended to be submitted to peer reviewed journals.

CHAPTER 2. BACKGROUND

This chapter is divided into relevant subtopics related to the human spine. The first section consists of basic information on the spine and the structures that make up the cervical spine. The second section details how the cervical spine moves. The third section introduces different methodologies for cadaveric *in vitro* testing.

The cervical spine is a vital structure for support, mobility and protection. Its primary function is to support the human head. The strength and flexibility of the spine enable it to act as a shock absorber to protect the brain. The complex joints and muscles allow a wide range of motion for head movement. It also serves to protect the spinal cord as it exits the brain (Nordin *et al*., 2001).

2.1 Spinal Anatomy

The human spine is composed of 33 vertebrae, intervertebral discs, and other soft tissue structures. The column is characterized by areas of curvature and vertebrae into the cervical, thoracic, lumbar, and sacrococcygeal regions. The cervical spine consists of 7 vertabrae, thoracic, 12, and lumbar,5, all of which are mobile. The sacrum is composed of 5 fused vertebrae and is fused to the coccyx which can have 4-5 fused vertebrae (Hamill *et al*., 2003). A spinal motion segment unit consists of adjacent vertebrae, the intervertebral disc between them, and ligaments connecting the vertebra.

The first cervical spinal body, C1, otherwise known as the axis, permits coronal rotation of the head. It is unique in that it has no vertebral body and is connected to the inferior C2 vertebra by the dens. This study pertains to the subaxial cervical spine, so the following sections will detail subaxial cervical spine structures. The subaxial spine is shown in **Figure 2.1**. The figure also includes the first thoracic vertebra (similar to the specimen used in the following studies). The lordotic curvature of the cervical spine is produced by the wedge shaped vertebral bodies.

2.1.1 Cervical Vertebrae

A typical cervical vertebra is shown from lateral and superior views in **Figure 2.2**. The largest structure by volume is the vertebral body. The vertebral body serves as the attachment point for the IVD and transfers a majority of the axial load. Extending from the body laterally are the transverse processes and poseteriorly are the pedicles. The pedicles connect to the lamina and spinous processes to create the vertebral foramen, through which the spinal cord passes. The superior and inferior zygoapophyseal or facet joints are located at the junction of the pedicle and lamina.

The vertebrae are characterized by their relatively small bodies and transverse processes, transverse process foramen, uncinate processes, and orientation of their facet

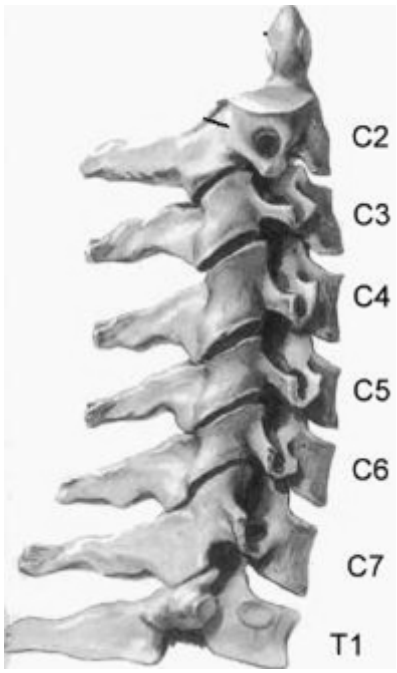

Figure 2.1. Subaxial cervical spine with T1 vertebra

Adapted with permission from Cervical-spine.org [Internet]. Denmark: Whiplash Connection; c2008-2011 [Updated 2010 Sep 20; cited 2011 Mar 10]. Available from: http://www.cervical-spine.org/index.php/Overview:_Head-neck-joint_instabilities.

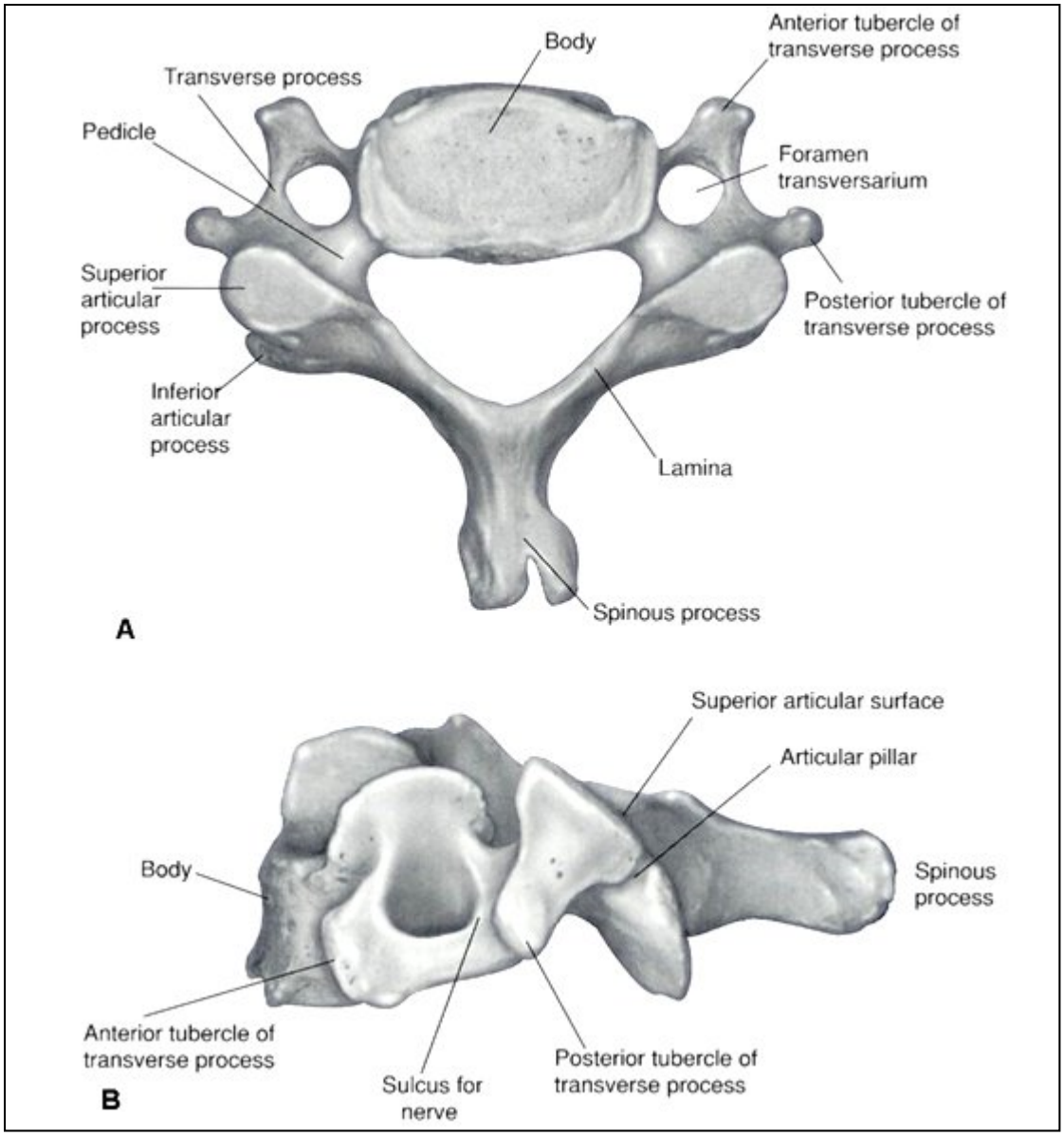

Figure 2.2. Cervical vertebra

Superior coronal (A) and left lateral (B) views of a cervical vertebra. Adapted with permission from Hochman M., Tuli, S. Cervical spondylotic myelopathy: a review. J Neurol [Internet]. 2009 Feb [cited 2011 Mar 10];4(1):[about 10 p.] Available from: http://www.ispub.com/ostia/index.php?xmlFilePath=journals/ijn/vol4n1/cervical.xml.

joints. The cervical vertebral body is smaller in size and more rectangular (wider than deep) than lumbar and thoracic vertebra. The transverse processes have foramen, foramen transversarium, which provide a passageway for the vertebral artery, vertebral vein, and nerves. The uncinate processes are unique bony prominences that emanate from the superior lateral aspects of the vertebral body from C3 to T1. Their interaction is known as Luschka's joint which limits lateral bending. Spine surgeons often use these as landmarks to prevent access to the nervous and vascular tissue passing through the foramen transversarium. Cervical facet joints are oval in shape and angled cranially 45° in the sagittal plane. When compressed, the facets help distribute the axial load (Nordin *et al*., 2001).

C2 and C7 have aspects that differ from the rest of the cervical vertebra. C2 has a process arising from the superior anterior portion of the vertebral body known as the odontoid process, or "dens". The dens protrudes through the C1 vertebra and serves as an axis for it to rotate about. The C2 vertebra is commonly referred to as the "axis" because of the functionality of the dens. C7 has the longest spinous process in the cervical spine. The spinous process is usually easy to palpate and has resulted in C7 being alternately labeled vertebra prominens.

2.1.2 Intervertebral Disc

The IVD is a significant part of the spinal joint complex. It lies between two adjacent vertebral bodies and serves as connective tissue for the spinal column, as well as, to absorb compressive and shear loads (White, *et al*., 1990). The IVD is an avascular, viscoelastic structure with two main regions and cartilaginous endplates. The outer ring of an IVD is the annulus fibrosus and the inner region is the nucleus pulposus. **Figure 2.3** shows a transverse cross section of an IVD in a MSU. Each component has a very low cell density. The cartilaginous end plates are mainly made up of chondrocyte-like cells that produce hyaline cartilage to cover their thin layer of cortical bone. The annulus fibrosus is populated by two types of cells. In the outer rings, it contains cells that resemble long fibroblasts and in the inner rings, cells that resemble rounded chondrocytes (Zao *et al*., 2007). The nucleus pulposus is constantly modified and as a result contains different cell types at different stages of life. From birth until the age of 4, the nucleus contains Notochordal cells. However, as they age, the notochordal cells disappear and the nucleus becomes filled with the chondrocyte-like cells similar to those in the inner annulus or cartilaginous end plates (Urban *et al*., 2000).

The annulus is composed of densely packed collagen type I fibril sheets. They are organized in a perpendicular manner with the cells seeded intermittently. The annulus is able to provide much of the load support due to its high composition of type I collagen. The nucleus contains significantly less collagen type I and instead its cells are seeded on a type II matrix (Zao *et al*., 2007). The nucleus also contains a large amount of proteoglycans.

Proteogylcans are heavily glycosylated gylcoproteins. Their main structure

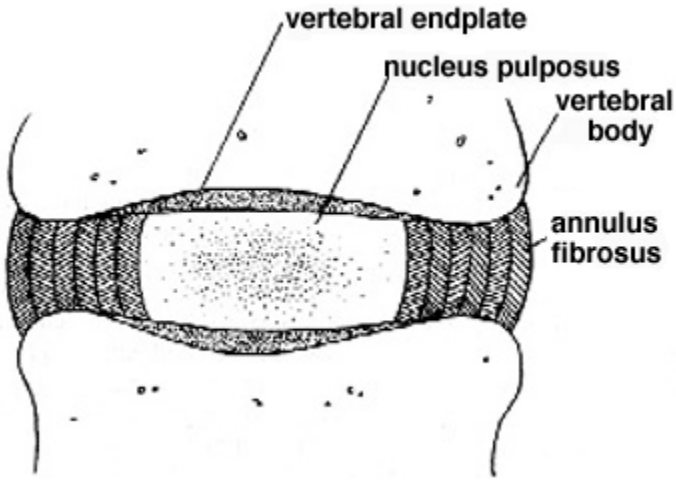

Figure 2.3. Intervertebral disc structures

Adapted with permission from Mcinerney J, Ball P. The pathophysiology of thoracic disc disease. Neurosurg Focus [Internet]. 2000 [cited 2011 Mar 10];9(4): [about 5 p.] Available from: http://www.medscape.com/viewarticle/405642_1.

consists of a core protein with glycosaminoglycan side chains. In most cases, after the mRNA sequence for the particular protein is translated into an amino acid sequence, it is modified in the rough endoplasmic reticulum and the Golgi apparatus by the attachment of oligosaccharides from dolichols and glycotransferases. In the IVD, aggrecan is the most common proteoglycan. Hyaluronate is the core protein and it is attached to glycosaminoglycan side chains of chondroitin sulfate and keratin sulfate (Alberts *et al.,* 2004; Chung *et al*., 2003; Zao *et al*., 2007).

The nucleus pulposus obtains its gel-like properties from its proteoglycan filled matrix. The chondroitin sulfate side chains on aggrecan establish a negative charge on the matrix (Urban *et al*., 2000). This negative charge attracts a large sodium ion concentration to balance the charge. This alters the osmolarity of the matrix, making it hypertonic, which causes water to flow inwards. This is also known as the swelling pressure. In young individuals, the nucleus can be 90% water, but with aging, the water content is reduced to 70%.

The importance of aggrecan and its contribution to a swelling pressure is equaled by the presence of collagen in order to counteract the influx of water. Collagen limits the size of the nucleus in order to prevent it from growing too much and physically tearing the surrounding connective tissue. The coordination between the proteogylcans, collagen, and water give the IVD its mechanical properties, while the chondrocytes and fibroblasts maintain the structures (Chung *et al*., 2003).

2.1.3 Ligaments

Ligaments are connective tissues that attach bones to other bones. They are made up of collagen, elastin, and reticulum fibers (Nordin *et al*., 2001). Two types of ligaments exist in the cervical spine: capsular facet ligaments and extracapsular ligaments bridging vertebral bodies. **Figure 2.4** shows the ligaments on a MSU. The capsular facet ligaments create a joint capsule around the facets and limit sagittal and axial motion. The anterior longitudinal ligament runs the length of the spine on the anterior aspect of the vertebral bodies and limits extension. The posterior longitudinal ligament runs the length of the spine along the posterior aspect of vertebral bodies, inside the vertebral foramen. The intertransverse ligament connects adjacent transverse processes and helps limit lateral bending and flexion. The ligamentum flavum connects adjacent segments and is located inside the vertebral foramen connected to the lamina. The ligamentum flavum serves to help limit flexion. The interspinous ligament connects adjacent spinous processes and the supraspinous ligament runs the length of the spine connecting all the spinous processes. Both ligaments serve to limit flexion.

2.2 Cervical Spine Kinematics

The cervical spine is capable of translations and rotations in all directions, giving it 6 degrees of freedom (3 translational and 3 rotational) (White *et al*., 1990). **Figure 2.5**

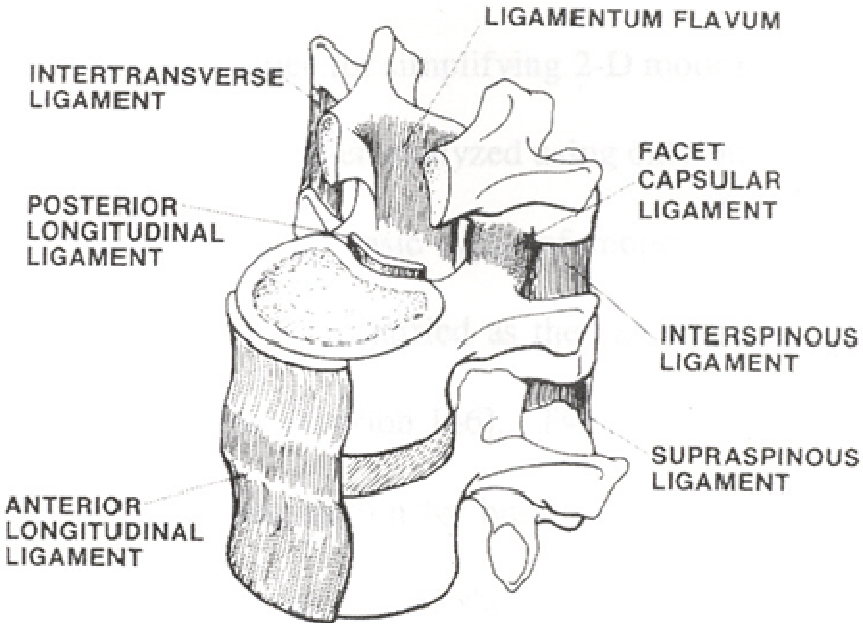

Figure 2.4. Spinal ligaments

Adapted with permission from White A, Panjabi M. Clinical biomechanics of the spine. 2nd ed. Philadelphia: J.B. Lippincott; 1990. p. 20.

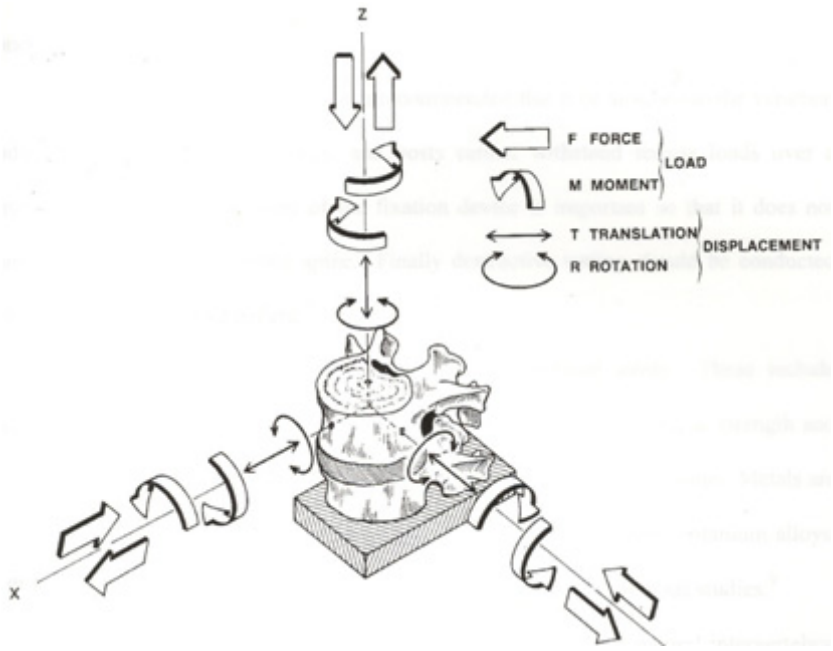

Figure 2.5 Degrees of freedom in a MSU

Adapted with permission from White A, Panjabi M. Clinical biomechanics of the spine. 2nd ed. Philadelphia: J.B. Lippincott; 1990. p. 54.

shows loads and displacements in a MSU. Forces directed antero-posteriorly (in the "X" direction) are called shear forces. Forces directed in the "Z" direction are called axial forces. The X-Z plane corresponds to the sagittal anatomical plane. Moments in the sagittal plane produce flexion and extension rotations. Moments in the Y-Z plane produce lateral bending. Moments in the X-Y plane produce axial rotations. Lateral bending and axial rotation are coupled motions due to the orientation of the facet joints. For example, a left lateral bend will induce a counterclockwise axial rotation.

2.3 Biomechanical Testing

The demand for biomechanical testing increases as new medical devices and surgical techniques are introduced. There are a wide variety of test frames and loading protocols to evaluate the clinical augmentations. They range from screw pullout studies involving a single actuator and a single axis load cell to complex 6 degree of freedom frames capable of performing coupled motions and high resolution force and moment measurements along each axis. Due to the high standards placed on evaluating a new device, one test in any frame is hardly sufficient to evaluate all of its characteristics (Goel *et al*., 2006).

Spinal biomechanical testing is generally categorized as either flexibility or stiffness testing. The flexibility protocol utilizes an input load and measures the displacement response. The stiffness protocol has a displacement input and the load is measured (Panjabi *et al*., 2007). Screw pullout testing and fixed axis testing (Bonin, 2006) are both stiffness protocols. The fixed axis protocol prescribes a center of rotation and rotates the specimen about the arc while measuring forces and moments. The most common flexibility protocol is the pure moment protocol. Additional protocols do not follow the "well defined" criteria established by Panjabi, but attempt to recreate more physiologic loading conditions. The eccentric loading protocol uses a displacement controlled actuator and fixturing to apply a bending moment and force to a spinal segment.

Robotic testing frames have aided in the development of advanced protocols. The Spine Robot is a 4 degree of freedom spinal biomechanical test frame. It has a wide range of testing capabilities and served as a platform to incorporate real time force control into biomechanical testing. Real time force control is a robotic control algorithm designed to maintain an end effector's contact force on a target. Industrial robots use force control in sanding and polishing applications (Gorinevsky *et al*., 2001). The Spine Robot used a force control algorithm to simulate the eccentric loading protocol (Kelly, 2005). It has also been used in fixed axis testing (Bonin, 2006) and to simulate quasi-static pure moment applications (Fraysur, 2009).

CHAPTER 3. USE OF A SPINE ROBOT TO SIMULATE AND COMPARE A PURE MOMENT PROTOCOL WITH AN ECCENTRIC LOADING PROTOCOL IN SUBAXIAL CERVICAL CADAVERIC SPINES

3.1 Introduction

Biomechanical testing provides a critical tool for understanding the load and motion response of the subaxial spine. Numerous testing methodologies and paradigms exist in the spinal biomechanics research community. Common standard protocols include pure moment (Fraysur, 2009; Kubo *et al*., 2003), pure moment with follower load, (Miura *et al*., 2002; Patwardhan *et al*., 2000) hybrid (Panjabi *et al*., 2007), and eccentric lever arm loading protocol (DiAngelo, Foley *et al*., 2003; DiAngelo, Scifert *et al*., 2003). The pure moment protocol applies a pure rotational moment to a free end of a spinal segment while the opposite end is rigidly fixed. A variety of methods of pure moment application have been reported, including: counterbalanced levers, pulleys, and sliding pulleys, as well as, controlled motorized methods (Egzubal *et al*., 2010; Goertzen *et al*., 2009; Kelly, 2005; Lysack *et al*., 2000). In addition to the moment application, the loading sequence also varies; some protocols use a quasistatic stepwise procedure to reach the moment end limit, whereas others are continuous. The follower load concept incorporated a compressive load throughout the spinal column to simulate muscle forces and body weight (Patwardhan *et al*., 1999). The hybrid protocol has been used to evaluate spinal instrumentation by measuring the motion response to a load limit in the intact condition and forcing the instrumented condition through the same range of motion (Panjabi *et al*., 2007). The EL protocol was produced by means of a vertical actuator applying a load to a lever attached to an inverted spine. In the EL protocol, a single actuator is connected to the lever through a frictionless slider bearing and rotational joint thereby applying a force and moment in a defined plane of movement (DiAngelo, Scifert *et al*., 2003). Many traditional protocols have relied on hanging dead weights, cable and pulley, and single linear actuators for load application. The varied end loading conditions in each protocol, differing strategies to apply the same loads, and stepwise versus continuous loading are variables that could affect the motion response.

Recently, industrial robotic concepts have been incorporated into biomechanical testing protocols (Gilbertson *et al*., 2000; Goertzen *et al*., 2009; Kelly, 2005). Robotic based testing platforms are capable of precise, coordinated motions, and high frequency and resolution load monitoring. One such platform is the Spine Robot for which real time force control algorithms have been developed (Kelly, 2005). Real time force control is a control technique widely used in manufacturing applications to maintain a targeted contact force or force profile between a robot and its environment. The control structure of the robot required a high frequency force feedback which modulated the motion output. Robotic sanding, grinding, or deburring are areas that utilize real time force control (Gorinevsky *et al*., 2001). In the spinal biomechanics community, real time force control implementation is far less common. In addition to the Spine Robot, the authors are aware of only one other published effort to incorporate real time force control into spinal biomechanical testing. Goertzen has developed an algorithm to control end loads

on sheep spines through the implementation of a jog function. However, work was limited to application of pure moment loads (null forces) to one rabbit single MSU (L3-L4) specimen.

Robotic based real time force control provides the potential to run continuous motion tests while maintaining desired end loads within a desired confidence interval. The ability to specify different targeted end load conditions would enable any *in vitro* biomechanical test to be simulated with a singular test platform. Although *in vitro* data are routinely compared between labs, regardless of the differences in protocols, we are unaware of any protocol comparisons using the same testing platform. Use of a consistent platform removes variables that differ from lab to lab such as fixturing weight, method of load application, and load and rotational measurements. The goal of this study was to use the Spine Robot to simulate a continuous pure moment protocol and to compare the results to that for our previously simulated EL protocol to determine the effects of varied loading conditions on the motion response of the subaxial cervical spine.

3.2 Materials and Methods

The following sections will detail the preparation and execution of spinal biomechanical testing. The process is broken down into: Specimen Preparation, the Programmable Robotic Testing Platform: Spine Robot, Force Control Algorithm, Testing Protocol, and Data Management.

3.2.1 Specimen Preparation

Six fresh sub-axial (C2-T1) human cadaveric spines were obtained (Restore Life USA, Johnson City, TN) and screened using antero-posterior and lateral radiographs to ensure normal spinal anatomy as illustrated in **Figure 3.1**. Specimens with motion restricting ossification, excessive intervertebral disc degeneration, or spinal injury were excluded from the study. Mean specimen age was 55.7 ± 11 years (4 male, 2 female). Excess musculature was removed with care to keep ligaments and discs intact. Exposed endplates of the cranial (C2) and caudal (T1) vertebral bodies were cleaned of all disc material and a series of screws were inserted for mounting in low melting point bismuth alloy. Care was taken to maintain the natural neutral alignment and lordotic curvature. Threaded rods were inserted into the spinous processes of C3-C7 for LED target attachment. A non-contact optical tracking system (Origin Instruments, Grand Prairie, TX) interfaced with a custom LabView VI (National Intruments, Austin, TX) measured LED target displacements and computed vertebral body rotations.

3.2.2 Programmable Robotic Testing Platform: Spine Robot

A previously developed programmable multi-axis robotic testing platform (Spine Robot) was used for the current study (Kelly, 2005). The 4 degree of freedom system

Figure 3.1. Lateral radiograph of potted spine

Spine is mounted in neutral upright position (C2 top). LED targets were attached to spinous process rods. For scale, the interior distance between the two nuts on the vertical rod is 10mm.

consisted of two orthogonal translational linear actuators (x, z axes) and two rotational motors (pitch, roll) capable of high resolution coordinated motion applied through a custom gimbal joint (positional resolutions: x: 2.0 μm, z: 0.31 μm, rotational: 0.0045°). Horizontal, vertical and curved arrows in **Figure 3.2** show the motions associated with the current study. The kinematic configuration of the Spine Robot permitted full coordinated control of global sagittal plane movements. Force and moment monitoring was provided by two 6-axis load sensors. The cranial end of each test specimen was secured to the first force sensor which remained rigidly affixed to, and moved with, the gimbal of the Spine robot. This sensor performed two functions: 1) measurement of all forces and moments applied to the caudal end of the test specimen and 2) provision of force feedback to the motion controller for real time path modification and force control. Because this sensor moved with the test specimen cranial end, transformation of the sensor reference frame to the C2 vertebra created a moving anatomical force reference system that measured (and controlled) cranial-caudal compression and anterior-posterior shear forces applied to C2 as it rotated in the sagittal plane (**Figure 3.3**). The second (caudal) force sensor remained rigidly fixed between the test platform base and caudal end of the test specimen and measured all transferred loads in a stationary world force reference frame.

3.2.3 Force Control Algorithm

A previously developed control algorithm was used that employed a real time trajectory path modification feature of the controller to modify a user programmed global C2 vertebra path in real time according to desired specimen end loading criteria (Kelly, 2005). The trajectory generator of the Spine Robot breaks down the user programmed path into discrete setpoints that are computed and updated at 4ms intervals. The real time path modification feature enabled user control of the individual 'setpoints' by superimposing a desired distance change in the z-axis (delta z) and x axis (delta x) directions. Delta z and delta x values were computed in 4 ms intervals by multiplying the force error (difference between actual current force and desired programmed force) by a proportional gain constant. The real time force control algorithm therefore depended on 3 aspects: 1) a predefined global trajectory of C2 as the input path, 2) force feedback and proportional gain setting and, 3) ability of robotic controller to modify path 'setpoints' in real time to delineate a global spinal path that met targeted compression and shear forces in the moving anatomical force reference frame. This method of force control was an iterative process. All spines started with a generic global path (modeled as a second order polynomial function) which was modified in real time based on the force feedback and setpoint modification to an initial rotational end limit of 5 degrees. The newly acquired path was recorded and applied to the next incremental global rotation. Rotations were incremented by 5 degrees, so by the testing end limit of 28-45 degrees, the specimen had been pre-cycled. A ± 5 N force error in shear and compression was targeted. If after 3 tests at the moment end limit, the specimen could not perform within the force error tolerance, the path with the least error was selected and analyzed. By programming different desired end load compression and shear values into this force control algorithm, different end load conditions throughout a full flexion-extension range of motion could

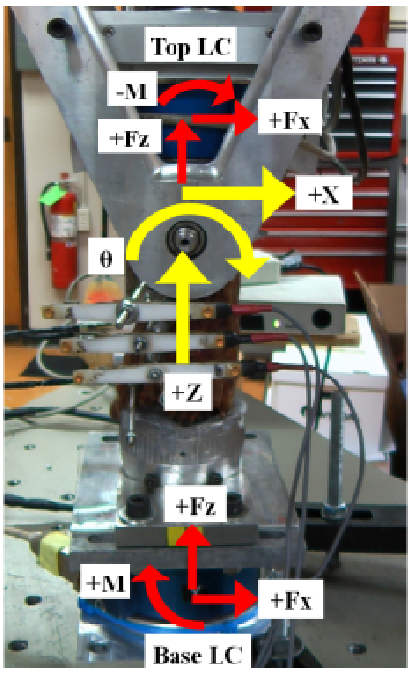

Figure 3.2. Test specimen setup

World coordinate system orientation (yellow) and force sensor coordinate frames (red).

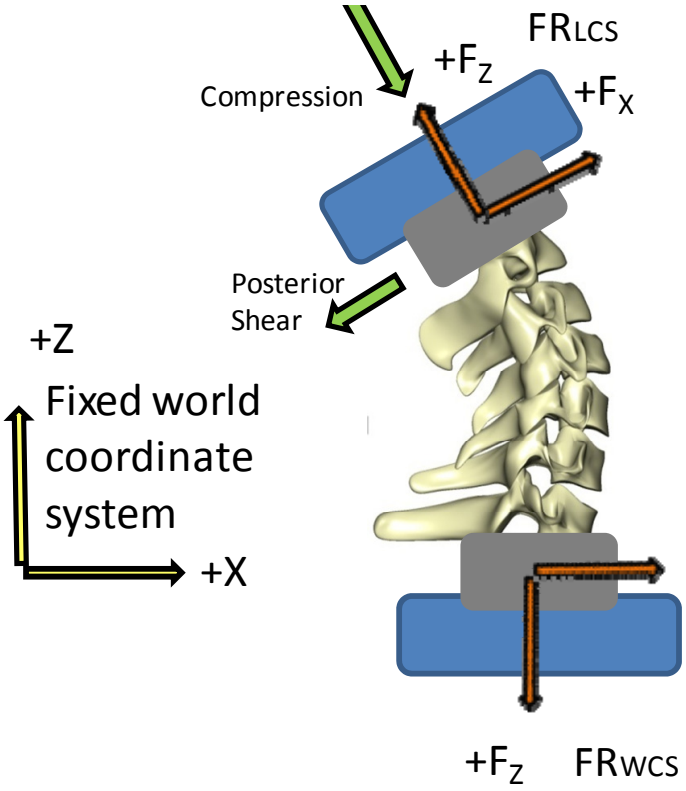

Figure 3.3. Schematic illustrating compression and shear force vectors

The forces are controlled by the robot through translations in the world coordinate system and read in a moving anatomical force reference frame (FR_{LCS}).

be achieved and hence different testing protocols simulated.

3.2.4 Testing Protocol

Previous work derived and modeled global compression and shear forces applied to C2 throughout a full flexion-extension motion range during testing with an eccentric lever arm (EL) protocol (DiAngelo *et al*., 2003; Kelly, 2005). Simulation of the EL protocol in the Spine Robot was achieved by programming modeled end load conditions (**Equations 3.1** and **3.2**) and employing the force control strategy described above.

$$Fz = 0.9M^2 + 3.4M + 20 \text{ (N)} \qquad \textbf{(Eq. 3.1)}$$

$$Fx = Fz*\tan(\theta) \text{ (N)} \qquad \textbf{(Eq. 3.2)}$$

Where:
M = current moment value [Nm]
Θ = current amount of global rotation [deg]
Fz = compressive force at C2 vertebra in moving anatomical force reference frame [N]
Fx = shear force at C2 vertebra in moving anatomical force reference frame [N]

In the current study, the above algorithm for control of global spinal end loads was modified to apply compression and shear forces that simulated a pure moment testing protocol. Programmed compression and shear forces were modified to static values as shown by **Equations 3.3** and **3.4**.

$$Fz = -5 \text{ (N)} \qquad \textbf{(Eq. 3.3)}$$

$$Fx = 0 \text{ (N)} \qquad \textbf{(Eq. 3.4)}$$

Each spine was tested using the simulated EL protocol, then removed, re-mounted and tested using the simulated PM protocol. Each spine was tested in flexion then extension to a non-destructive 3 Nm bending moment. All testing was carried out in room temperature conditions and specimens were moistened before flexion, between bending modes, and after extension (20-30 minute intervals).

3.2.5 Data Management

Robot translations and rotations, applied cranial forces and moments, transferred caudal forces and moments, and individual vertebral body translation and rotations were recorded for all tests. Force control performance and confidence interval maintenance was quantitatively evaluated by plotting the difference between the target force and actual force versus global rotation. Graphs of programmed (desired) spinal loads subtracted from experimentally applied spinal loads were generated to evaluate force control performance. Deviations from 0 indicated “force errors”. A ± 5 N force error was desired

for testing, thus indicating the end loads were consistent with the protocol demands. Flexibility curves for the EL and PM tests were inspected for a difference in general loading patterns. The pure moment protocol was evaluated by comparing the applied (cranial) flexibility curve to the transferred (caudal) flexibility curve and statistically comparing global end moment values. Motion segment unit (MSU) rotations were calculated by subtracting the rotations of two adjacent vertebral bodies. MSU percent contribution to global rotation was calculated by dividing individual MSU rotations by the global rotation. MSU percent contribution was compared at each level between the EL and PM protocols using a paired T-test ($\alpha = 0.05$).

3.3 Results

The following section describes the results from the protocol simulations. It is broken into Loading Verification and Motion Response sections in order to first demonstrate the ability to simulate each protocol, then analyze the actual protocol differences.

3.3.1 Verification of Loading Conditions

3.3.1.1 Force Error. Force errors are the difference between the measured force and the force targets defined by **Equations 3.1** to **3.4**. Sample force error graphs for the EL and PM simulations are shown in **Figure 3.4**. A positive error indicates a tensile axial or anterior shear force error. A negative error indicates a compressive axial or posterior shear force. Initial force errors at the onset of testing caused by mounting or tissue relaxation tended to quickly correct. The force was relatively well controlled through most of the range of motion. The intermediate force error profiles tended to be gradual with very small amplitudes of oscillation. Some had a slight drift in the force error that typically stayed within 3 N of the target. In flexion, a 3-5 N spike occurred within the first 15° of motion. Within 3°-5° of the global end limit of rotation the force error was difficult to control. In flexion, the axial force error changed rapidly, but was well maintained around 0. In extension, the axial error increased rapidly, but tended to be unidirectional. The maximum axial error was 6.1 N. Since the algorithm corrected the large peak errors, the average terminal error was 3.6 N at the moment end limit where comparisons were made. The shear force errors in both flexion and extension exhibited similar error profiles compared to the axial loading results, but at a much smaller magnitude. The maximum shear force error that occurred over all testing was 4 N. **Figure 3.4** demonstrates intermediate error in flexion at 5 and 10 degrees and slight initial shear error.

3.3.1.2 PM Cranial Moment versus PM Caudal Moment. Sample global flexibility curves generated from the cranial and caudal load cell for a PM test are shown in **Figure 3.5**. The comparison of the cranial load cell (applied moments) with the caudal

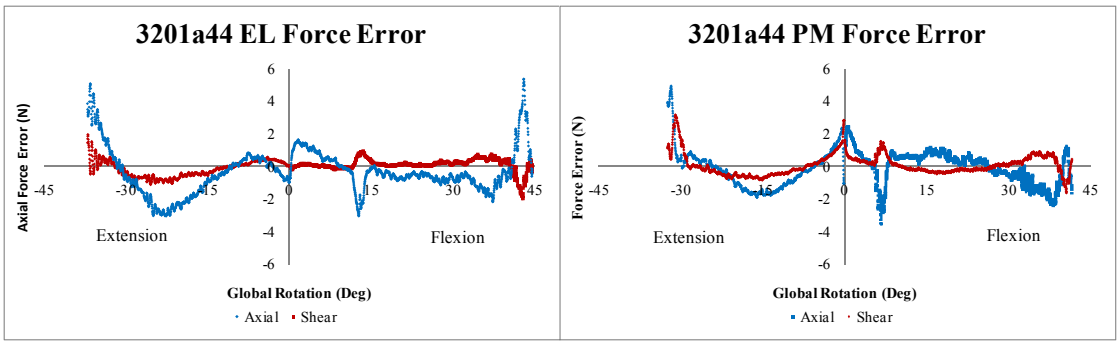

Figure 3.4. Force error summary

Shear and axial force errors for the eccentric loading and pure moment simulations in flexion and extension.

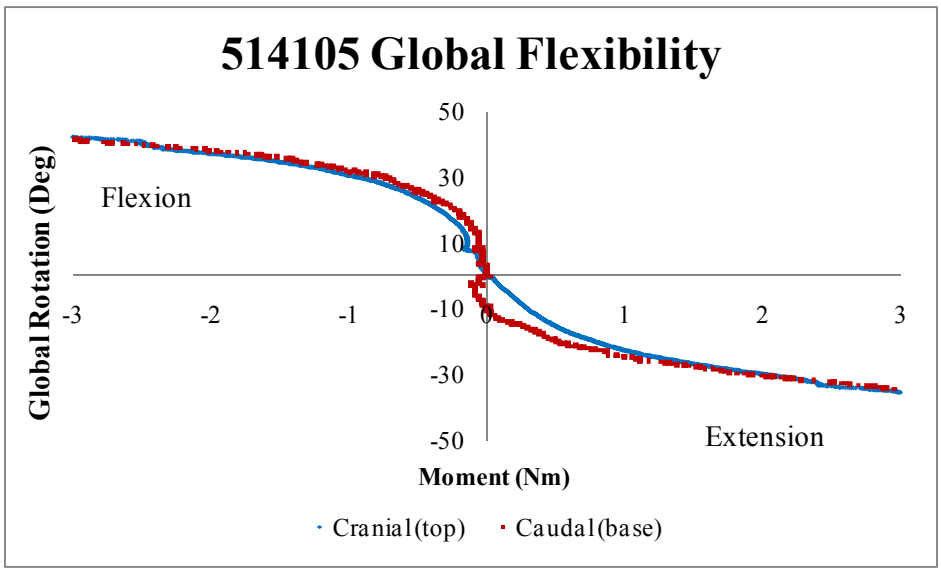

Figure 3.5. Global flexibility curves for caudal and cranial load cell

load cell (transferred moments) shows that applied moments (read from cranial load cell) were consistent with the transferred moments (read from the caudal load cell). Visually the curves compare extremely well. The average final moment end limit for the cranial load cell was 3.002 Nm, while the average final moment end limit for the caudal load cell was 3.0085 Nm. A paired student t-test ($\alpha = 0.05$) did not detect a significant difference between the cranial and caudal load cell values.

3.3.2 Motion Response

3.3.2.1 Percent Contribution to Global Motion. The mean MSU percent contribution to global motion profiles for the both the EL and PM simulations are shown in **Figure 3.6**. The only significant differences that occurred in the MSU motion response between the EL and PM protocols were found at C6-C7 in flexion and C7-T1 in extension. The most mobile MSU for flexion and extension was C5-C6 in both protocols. Combined, flexion plus extension, mean MSU percent contribution to global motion is shown in **Figure 3.7**. No significant differences between the two testing methods were found at any MSU.

3.3.2.2 Segmental Recruitment. Individual vertebral body rotations were tracked and relative motions were calculated throughout the duration of the test. Using a normalized time scale, absolute MSU rotations were plotted in order to visually compare the rate of segmental recruitment. **Figure 3.8** shows the segmental recruitment from each protocol for each MSU in flexion and extension. The graphs show the similar rates at which each MSU was recruited. These loading profiles were consistent with all testing.

3.3.2.3 Flexibility. Sample global spinal flexibility curves as recorded from the cranial load cell are shown in **Figure 3.9**. Both curves demonstrate the same general loading pattern and are representative of the entire dataset. These curves are consistent with other published data and demonstrate typical regions of nonlinear stiffness. The 2D simulation had 40.02° (SD = 7.3) of global flexion rotation and 36.8°(SD = 5.9) of global extension rotation. The PM simulation had 38.54° (SD = 7.3) of global flexion rotation and 34.63° (SD = 7.3) of global extension rotation. Global combined flexion + extension and independent flexion and extension showed no significant differences between the two protocols.

3.4 Discussion

A previous *in vitro* study using 6 subaxial cervical spines tested and compared the actual EL protocol and the EL simulation in the Spine Robot (Kelly *et al*., 2011). The study did not find significant differences in the motion response between the actual EL protocol and the EL simulation. These results served to validate the ability of the spine

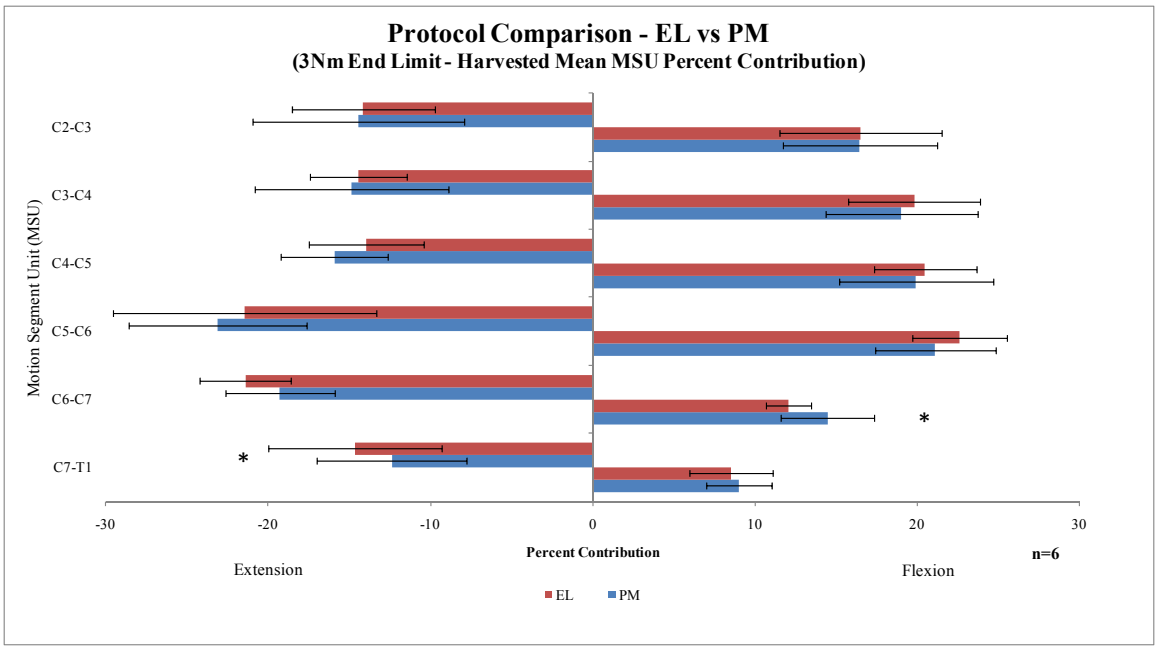

Figure 3.6. Flexion and extension mean segmental percent contribution to global rotation

Simulated eccentric loading protocol and pure moment protocol end limit motion segment unit percent contribution to global motion. Significant differences were observed between the two protocols and are indicated by an "*".

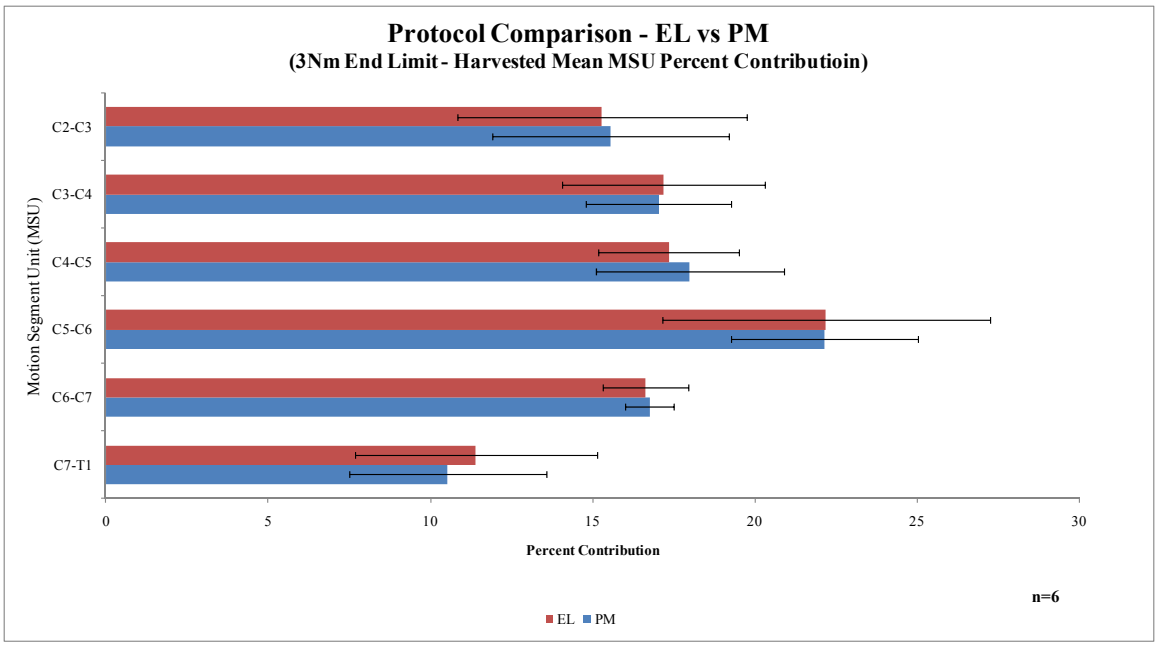

Figure 3.7. Combined flexion plus extension mean segmental motion contribution to global rotation

No significant differences between the simulated eccentric loading protocol or pure moment protocol were found.

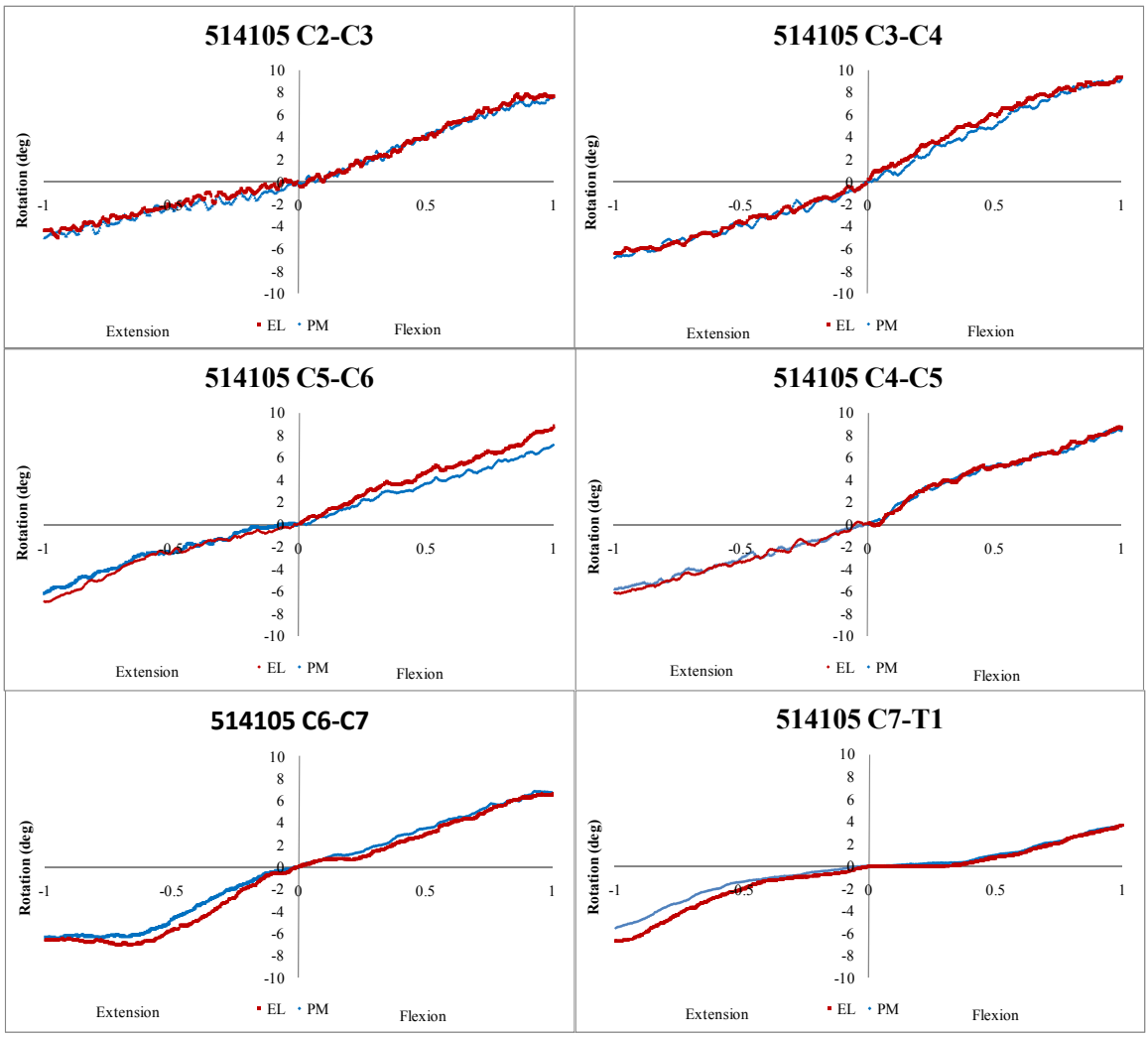

Figure 3.8. Segmental recruitment graphs for eccentric loading and pure moment simulations

Absolute motion segment unit rotation plotted versus a normalized time scale for flexion and extension for the simulated eccentric loading and pure moment protocols.

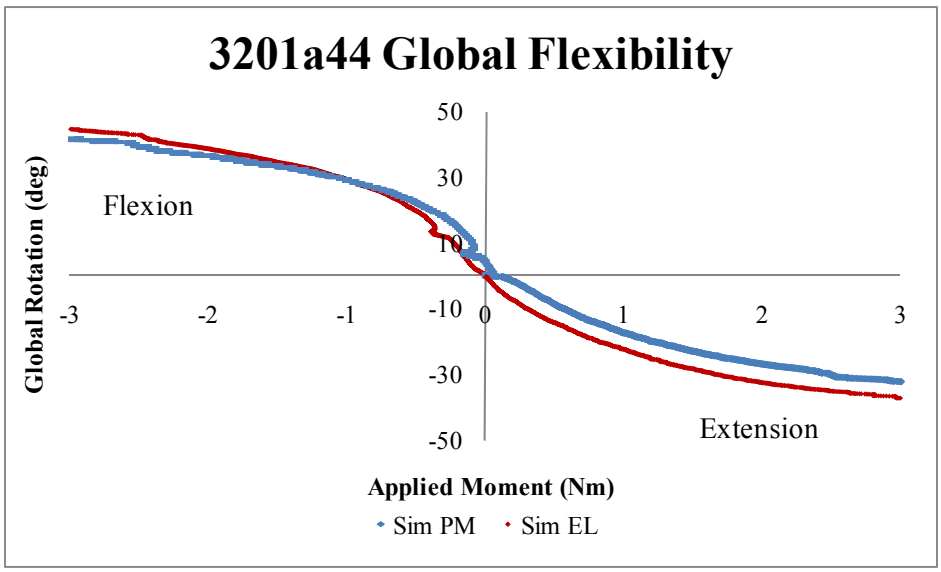

Figure 3.9. Sample global flexibility curves

Sample flexion and extension global flexibility curves for the simulated eccentric loading and pure moment protocols.

robot to replicate the end loading conditions of an existing standard biomechanical *in vitro* test protocol. The objective of this study was to directly compare the simulation of two different existing standard spinal biomechanical testing protocols, the EL protocol and a PM protocol. The consistency in fixturing, specimens, load application, and analysis provided a direct means of comparing the motion response due to two different end loading conditions. As indicated by the results, there was little significant difference between the simulated EL and PM protocols.

3.4.1 Verification of Loading Condition

It is important to address the issue of targeted loading compared to actual loading to confidently report end loading profiles. This task was simplified using the spine robot, because the applied force was determined based on data read from the cranial load cell. Since the cranial load cell's force reference frame moved with the local specimen force frame, the axial and shear forces read by the load cell directly correspond to the axial and shear forces applied to the spine. The force control algorithm corrected the global spinal path due to deviations from the commanded force. As described by equations 1 and 2, the commanded force increases as a function of moment to simulate the end loading conditions of the EL protocol. **Equations 3.3** and **3.4** show how static values are commanded for the PM simulation. The actual force errors at each point were calculated to see how well the system maintained the 5 N force error target. The force error profile shown in **Figure 3.4** is representative of the entire dataset. Overall, the maximum end limit-stiffness error was 6.1 N (peak), with a 3.6 N average terminal error for all tests. The low max error and consistently low errors throughout the test give the researchers confidence the desired loading conditions were being applied.

The pure moment protocol provided a second method of loading verification. The platform design incorporated a fixed caudal load cell, which allows for the transferred forces and moments to be monitored at the base of the specimen. The transferred moment was a good indicator for evaluation of the algorithm. In the PM protocol, the transferred moment theoretically should be equal to the applied moment. **Figure 3.5** shows the two similar stiffness curves. Typically, at each rotational increment the measured applied and transferred moments were close. The extension flexibility curves in **Figure 3.5** demonstrate a slight discontinuity. It is hypothesized that a small flexion moment was induced by the net effect of the preload and position of the specimen within the pot. The caudal (bottom) load cell reads forces and calculates moments based on its natural reference frame. Positioning the center of the spine anterior to the center of the load cell will result in a flexion moment when a compressive axial load is transferred through the spine. In the event additional unaccounted forces were acting on the spine, it would be expected that the transferred moment at the base would be affected. Despite the difference in moment, the compressive force effect was reduced as the specimen rotated, and at the end limit of rotation, the final moment values were similar. The average final moment values were 3.002 Nm for the cranial load cell and 3.0085 Nm for the caudal load cell. Furthermore, a paired t-test did not determine the values to be significantly different. The consistency of moment values measured with the cranial and caudal load

cells as well as the low levels of force error give the researchers confidence that the EL and PM protocols were accurately simulated.

Although the protocol was effective in simulations, several challenges prevented perfect force control tests. Testing could take 5-10 iterations for each mode of bending because the testing process utilized an iterative force optimization method. The method of prescribing a general path and allowing the Spine Robot to make adjustments to the path had two sources of error: specimen dependent and path dependent. Specimen dependent errors were due to the nonlinear stiffness characteristics of cadaveric tissue and the speed of the Spine Robot's response. The force errors were also influenced by the ability of the preprogrammed path to delineate the desired applied end load conditions. In situations where the programmed path closely mirrored the natural spine path, little to no modifications were required and the force error was very low. From a neutral position to the global bending end limit, three general areas of force error were realized: initial mounting error, intermediate error, and end limit-stiffness error. The initial mounting error was minimized by monitoring the forces and moments during the mounting process and moving the specimen to alleviate any force or moment. These errors were the least difficult for the Spine Robot to accommodate. As shown in **Figure 3.4**, the force error drops quickly from its non-zero starting position, generally within the first 5 degrees of motion. The relative laxity of the spine near the neutral position coupled with the high gain settings resulted in the effective force correction. The nonlinear mechanical behavior of cadaveric tissue results in varied zones of stiffness. One possible source for the intermediate errors is the change in stiffness. The force control algorithm gain settings were lowered with increasing bending moment values to maintain stability. Intermediate errors could be due to a non ideal curve fit as the curves are defined by a 2^{nd} order polynomial. The end limit stiffness errors were the most difficult to control and most important to regulate as the data was compared at 3Nm. The combination of the highest loads, greatest stiffness rate of change and lowest gain values presented a challenging force control climate. In flexion the terminal axial force errors typically had a rapid increase in tensile error followed by a similarly quick force correction. The highest "peak error" (defined by the largest pre-corrected force error) was 6.1 N while the average terminal error was 3.6 N. In addition to the robot response, errors were optimized by re-running the test with updated path functions and modified gain values. The low levels of force error show how the force control algorithm was effective in controlling the end loads.

3.4.2 Protocol Comparison: Simulated EL versus Simulated PM

Our analysis of the two protocols included comparisons of the end limit absolute global rotations, MSU percent contributions to global rotations at the end limit, and an analysis of segmental recruitment which was made possible through the use of the real time force control algorithm.

The lack of significant differences between the MSU percent contribution to global motion in the EL and PM protocols was surprising based on previous studies. With

only C6-C7 showing a difference in flexion and C7-T1 showing a difference in extension the two protocols cannot be considered different. Furthermore, the combined flexion and extension data lacked any levels of significance. The similarity in protocols could be a result of the viscoelastic nature of human tissue. The question arises as to whether or not there are zones of acceptance for each of the commanded force profiles instead of a tightly defined global path. This would suggest input loads might not have differed enough to produce a different end limit motion response. Furthermore, a qualitative analysis at 1.5 Nm again produced similar motion profiles.

Despite a lack of difference in the end limit analysis, the possibility remained that the different end load conditions tested here in recruited MSUs in a different sequence. Since each protocol was continuous, the rotations for each MSU could be qualitatively compared at any global rotational or moment limit. The segmental recruitment rates as seen in **Figure 3.8** did not appear to deviate much between the PM and EL simulations past a certain point corresponding to 1 Nm of bending. After this point each level was recruited at the same rate and provided a similar motion contribution from each MSU.

3.4.3 Simulated PM Testing versus Traditional PM Testing

The possibility of improper loading from the Spine Robot and the nature of cadaveric tissue testing as potential reasons for the similarity of the two protocols has been addressed. The final area of consideration is comparison of the new data to previously reported data for the same testing protocol from other research laboratories. In searching the literature no *in vitro* studies reporting separate flexion and extension pure moment cervical motion profiles were found. Further complicating the literature review, most cervical spine studies only reported specific MSUs or tested incomplete cervical spine sections. The only PM dataset found for comparison to our simulated PM data was that reported by Kubo, *et al,*2003. Using combined flexion and extension data, **Figure 3.10** shows the segmental motion response in the Kubo study and in this study.

The simulated PM protocol consistently produced the most motion at C4-C6, while Kubo, *et al,* 2003. report the most motion at C3-C4 and C6-C7. Their combined flexion and extension profiles have a characteristic dip at the levels where the robot simulated PM generated the most motion. Their profile is similar to other labs using follower loads, but for direct protocol comparison, standard pure moment testing was considered only. A difference between our simulated pure moment protocol and the typical pure moment protocols performed elsewhere is the fact that our test specimens were constrained laterally. The effect of the constraint was minimized through positioning the specimen with no lateral shear force during the mounting procedure. Despite the lateral constraint, our method of specimen mounting may actually provide a more accurate motion analysis. The specimen is mounted in a neutral upright starting position that is precisely defined by the Spine Robot and maintained throughout testing. After the spine is flexed or extended it is returned to its starting position, whereas a free loaded specimen end can shift positions. The positional shift may in turn recruit

structures differently and affect the motion response of the spinal column. An added benefit of the setup was that flexion and

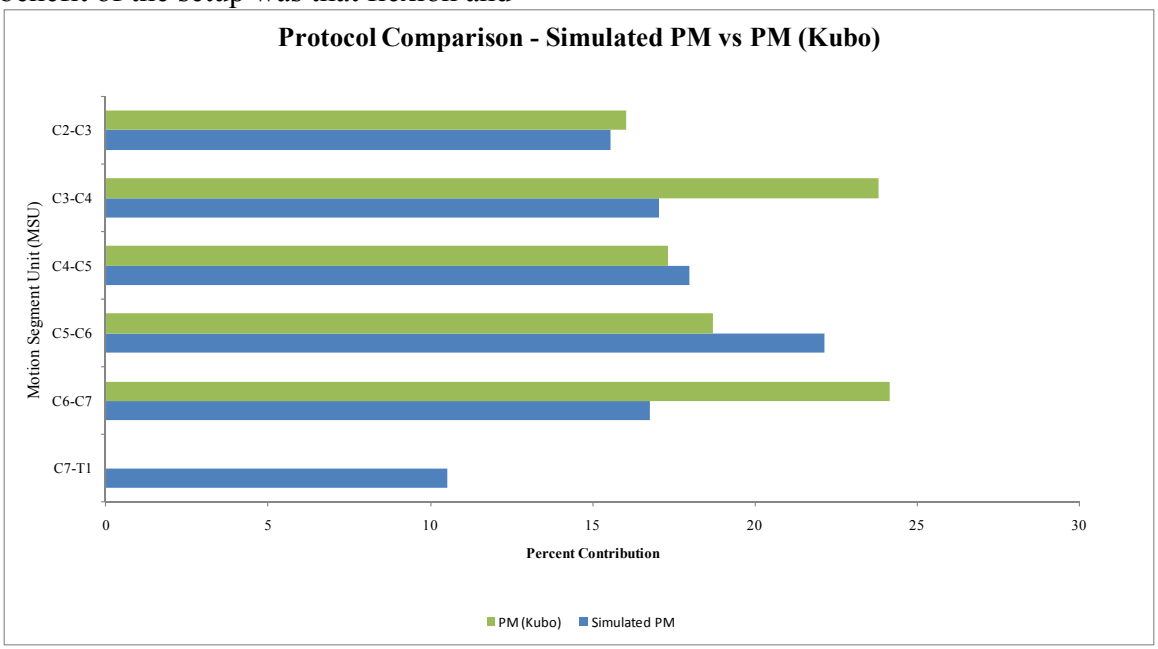

Figure 3.10. Published traditional pure moment motion response compared to simulated pure moment motion response

Mean motion segment unit combined flexion and extension percent contribution to global motion. Traditional pure moment from Kubo, *et al,* 2003, compared with the simulated pure moment protocol.

extension could be separated and analyzed individually where as other protocols are limited to a combined analysis.

Additional differences between our PM protocol and other reported PM protocols include the number of MSUs involved and the moment end limit. Often researchers use C2-C7 cervical spines (Kubo *et al*., 2003). Our protocol included the use of C7-T1. The additional motion segment could account for increased rotation, but in terms of segmental involvement should not drastically affect the general motion profile. Additional analysis on our rotational data indicated that the shape of the motion profile of **Figure 3.7** was not significantly altered when analyzed at a lower moment end limit of 1.5 Nm. The PM protocol at 1.5 Nm reported by Kubo demonstrated 46.8 degrees of combined flexion and extension global rotation using C2-C7. In comparison, our PM protocol averaged 73.1 degrees and our EL protocol averaged 76.8 degrees of global combined rotation. The consistency of our protocol and resulting motion profiles combined with the accuracy of our applied loads suggest the motion differences are a result of differing test setup not variations in the application of the simulated PM protocol. Limitations with standard protocols may also affect the reported pure moment motion profiles. Different methods of mechanical application of pure moments to the free end of a spine may induce unintended loads and influence the motion profile. The cable and pulley system is susceptible to the addition of force vectors due to the fixture weight and non-parallel cables in rotated positions (Eguzabal *et al*., 2010). Counterbalanced lever arm protocols similarly have the task of eliminating any fixturing preload. Even if the spines are properly loaded, non robotic methodologies have difficulty executing consistent continuous loading protocols. Stepwise loading is susceptible to testing artifacts. Goertzen et al demonstrated that the neutral zone increases in quasi static testing thereby increasing the overall range of motion of a porcine spinal column (Goertzen *et al*., 2004). In their study, the time between increments was 30 seconds, a value that can be even greater depending on the setup. Stepwise loading can also affect the viscoelastic tissue response depending on the number of steps the protocol takes to reach its moment end limit. As seen in Goertzen's study as well as numerous others, moment application is often broken into a series of 4 equal steps to reach the end limit (Miura *et al*., 2002).

3.5 Conclusion

The Spine Robot is a multifunctional biomechanical test platform capable of simulating different protocols. A simulated PM protocol did not significantly differ from a previously validated simulated EL protocol. Additionally, the simulated PM protocol motion response differed from a previously reported PM motion response. It is hypothesized that difference may be due to pure moment application not necessarily the end loading conditions. The Spine Robot is a powerful tool for spinal biomechanical testing. Its ability to perform *in vitro* testing with quasi-static load control, kinematic (fixed axis) and real time load control enable it to simulate virtually any loading scenario and serve as a platform for the development for new, more complex protocols. Development is underway for more physiologic loading scenarios, with the ultimate goal to replicate *in vivo* motion responses and recruitment rates.

CHAPTER 4. USE OF A SPINE ROBOT EMPLOYING REAL TIME FORCE CONTROL TO DEVELOP AND SIMULATE A HEAD WEIGHT INFLUENCED BENDING PROTOCOL

4.1 Introduction

In vitro test methods provide a vital tool for investigating the biomechanical behavior of the spine. The ultimate goal of *in vitro* spinal biomechanical testing is to replicate *in vivo* physiologic loads and motions. Numerous kinematic studies of the cervical spine can be found, however the cervical spine loads are largely unknown. *In vivo* load characterization is a very invasive process while a range of diagnostic imaging techniques can be used to measure spinal rotation. Since most biomechanical labs are not able to run clinical studies along with biomechanical benchtop studies, the main comparator between *in vivo* and *in vitro* data has been rotation from flexibility testing.

Traditional flexibility testing uses a known load as an input and measures the rotational output. Commonly, the Pure Moment (PM) protocol has been used for *in vitro* testing where a pure rotational load is applied to the free end of a spinal construct. No additional sagittal plane forces are applied in a true pure moment test.

Researchers have developed additional protocols to try to account for muscle forces and head weight with hopes of producing more *in vivo* motion responses. Some groups have utilized pure moment testing with an addition of a follower load, whereas others have used an eccentric loading (EL) protocol (DiAngelo, Foley *et al*., 2003). The EL protocol was designed to create a bending moment distribution along the spine. It utilizes a single vertical actuator with a slider bearing attached to a lever arm connected to the spine. The unique aspect of this protocol was that the spine was mounted with the caudal vertebral body on top and the cranial body affixed to the base. This mounting orientation subjects the cranial body to a lower moment than the caudal body, much like the *in vivo* scenario, where the lordosis of the spine causes a similar distribution due to the weight of the head. The follower load concept has been widely published by Panjabi, 2001, and Patawardhan, 2000. The distinguishing feature of the follower load protocol is the addition of cables and hanging dead weights in an attempt to produce a loading vector normal to each of the vertebral bodies throughout the range of physiologic rotations. The increased axial compression is intended to better simulate physiologic loading. While these protocols have been accepted, they have not demonstrated optimal correlation to published *in vivo* flexion and extension rotations. Furthermore, virtually none of the published studies attempt to investigate flexion and extension separately in order to fully evaluate the protocol.

The main limitation of the follower load is that the “physiologic load” is applied normal to each vertebral body as a compressive force. However, the *in vivo* load has a component of shear force as well as compressive force. In theory, the load should pass through the center of rotation (COR). It has been demonstrated that the MSU COR does not remain fixed. The follower load protocol makes an assumption as to the location of

the COR and passes the load through the point throughout the test. Another limitation of the follower load is that it is limited to only flexion and extension. The most basic biomechanical parts of the human head and neck are the vertebral bodies comprising the structural column support and the head which produces a vertically maintained force vector from head weight. **Figure 4.1** shows the head in a flexed position with the head weight force vector illustrated as the larger arrow. The head weight vector is resolved upon the C4-C5 intervertebral disc (IVD) to show components of axial compression (normal to the disc) and shear force (directed parallel to the disc). The head weight force vector is always a component of the net force along the spine, regardless of muscle activation. Therefore, biomechanical testing methods should incorporate this force in order to generate a shear force as well as compressive forces at each MSU level as occurs *in vivo*. No published literature has approached the study of cervical spine kinematics with a loading scenario isolating the effects of a vertical head weight force.

The purpose of this study was to use a Spine Robot to develop a real time force control based testing protocol to simulate cervical spine flexion and extension rotations under the influence of a vertically oriented head weight load. The physiologic head weight influenced loading (HWL) protocol assumes a 65 N force vector to model the force on the spine due to head weight. The Spine Robot is an advanced biomechanical testing platform that enables modification of pre-existing routines for the development of novel loading scenarios. Additionally, the Spine Robot enables individual flexion and extension analysis and thus more comprehensive comparison to *in vivo* studies with a similar breakdown. It is hypothesized that the higher end loading conditions from the HWL protocol will cause a varied motion response in comparison with established *in vitro* testing protocols.

4.2 Materials and Methods

4.2.1 Specimen Preparation

Six fresh human cadaveric spines (C2-T1) were screened using antero-posterior and lateral radiographs to check for motion restricting osteophytes and excessive disc degeneration. Mean specimen age was 55.7 ± 11 years (4 male, 2 female). Spines were prepared for testing by removal of excess musculature and disc material from exposed endplates, and insertion of screws into the endplate for potting fixation. Spines were then fixed in bismuth alloy pots with the superior aspect of the C2 body relative to a horizontal datum plane, while maintaining the natural lordotic curvature of the cervical spine. Threaded rods were then inserted into the spinous processes C3-C7 for non-contact motion tracking target placement.

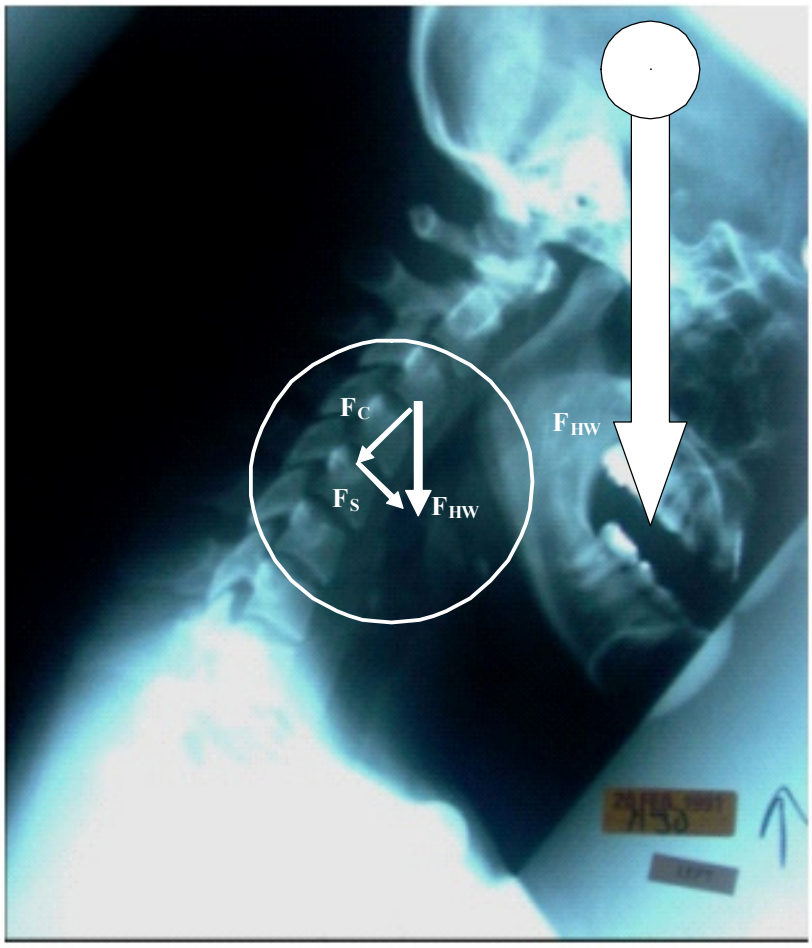

Figure 4.1. Lateral flexion radiograph

Head weight force vector F_{HW} illustrated by the larger vertical arrow originating at the assumed center of mass for the head. In the circle, the head weight force vector, $F_{HW,}$ is resolved at the C4-C5 disc, illustrating components of axial compression force, $F_{c,}$ and shear force, F_s.

Adapted with permission from CEEssentials.net [Internet]. Arvada,CO: TheNewPush, LLC; c2004-2011 [updated 2006 Aug; cited 2011 Mar 10]. Available from: http://www.ceessentials.net/article22.html.

4.2.2 Spine Robot

The previously developed Spine Robot consisted of 4 degrees of freedom (2 translational, 2 rotational) arranged in a gimbal configuration. The translational axes were fixed orthogonally, controlling axial and shear forces on the spine. The two rotational axes were configured to produce axial rotation and sagittal plane rotation (only sagittal plane rotation was used in this study). Forces were monitored with two 6-axis force and moment sensing load cells. One load cell was mounted to the gimbal assembly and attached to the mobile end of the potted specimen (cranial load cell). The other load cell was fixed to the base of the test frame (caudal load cell). The cranial load cell moved with the cranial vertebral body thus providing a moving local force reading frame. The caudal load cell remained fixed and its force reading frame remained aligned with the global positional coordinate system (**Figure 4.2)**.

4.2.3 HWL Protocol

A modification of the iteratively optimized real time force control protocol (Kelly, *et al.,* 2011) allowed for a 65N vertical load to be maintained throughout testing. The Spine Robot was programmed to modify end load targets as a function of sagittal rotation.

$$Fz = 65*\cos(\theta)\ (N) \qquad \textbf{(Eq. 4.1)}$$

$$Fx = 65*\sin(\theta)\ (N) \qquad \textbf{(Eq. 4.2)}$$

Where:
Fz = compressive force at C2 vertebra in moving anatomical force reference frame
Fx = shear force at C2 vertebra in moving anatomical force reference frame
N = Newtons
Theta = current amount of global rotation

Each spine was tested in flexion and extension to a non-destructive 3 Nm end limit with the HWL protocol. Testing was performed at room temperature and spines were moistened before testing, between bending modes, and after testing.

4.2.4 Data Management

Translations and rotations of robot axes, vertebral body translations and rotations, and forces and moments from each load cell were recorded for each test. End loads were verified by assessing the force error (difference between the commanded cranial force and the actual cranial force) for each mode of bending in all specimens. Force errors of 0 indicate perfect control of the forces. A ± 5 N force error limit was desired for testing. Motion segment unit (MSU) rotations were calculated from the non-contact tracking data by subtracting the rotation of a vertebral body from its caudally adjacent body. MSU

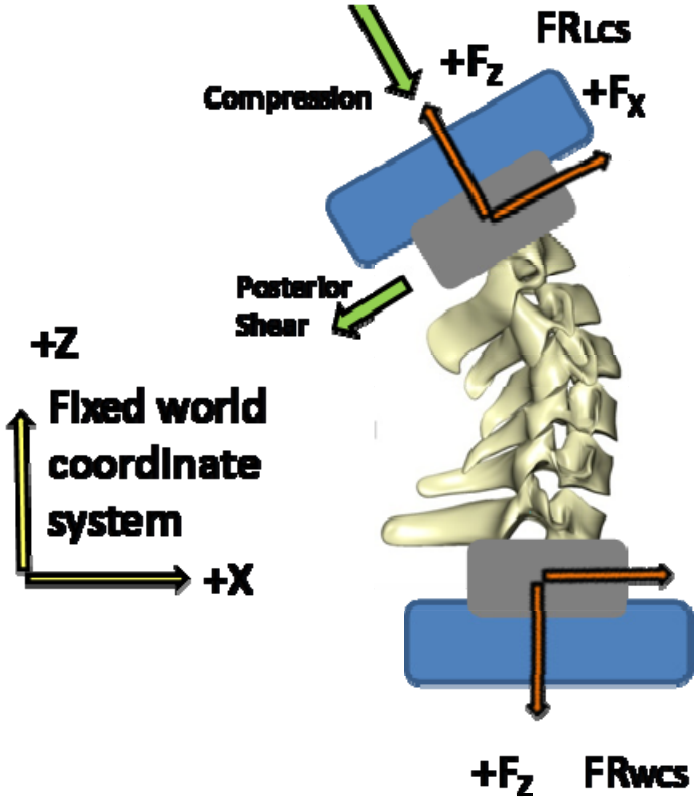

Figure 4.2. Local moving force reference frame and fixed world coordinate system

rotations were used to calculate segmental percent contribution to global motion by dividing the MSU rotation by global rotation. Data were analyzed in separate flexion and extension percent contributions, as well as combined flexion and extension MSU percent contribution to global motion. Motion data for all MSU levels were compared to those previously reported for the same specimens using robotic simulation of PM and EL protocols (Wido, 2011).

4.3 Results

This section will discuss the results obtained from running the HWL protocol. To ensure proper testing, the end loading conditions were first verified. After verification, the motion response of the spinal segment was analyzed.

4.3.1 Preload

The mean shear buildup was 6.35 N at the 65 N compressive preload limit. Initial moment values varied from 0.936 Nm to 2.5 Nm with a mean of 2.13 Nm. The motion tracking system was not used to monitor initial MSU rotations during preloading. No significant "buckling" effects were witnessed.

4.3.2 Verification of End Loads

Since the HWL protocol has higher end loads than the EL or PM simulation, the force control performance was evaluated. The force targets were functions of rotation in order to maintain a vertical 65 N force vector. **Figure 4.3** shows the targeted and applied loads for a sample extension test. The actual force error for the particular test is shown in **Figure 4.4**. These curves are indicative of the entire dataset. The average peak error in flexion was 2.15 N of shear error and 5.1 N of axial force error. The average peak error in extension was 1.62 N of shear error and 8.31 N of axial error. The average terminal error at the 3Nm end limit was 1.01N of shear and 4.32 N of axial force error in flexion and 0.84 N of shear and 6.81 N of axial force error in extension.

4.3.3 Motion Response

The mean range of motion for the HWL protocol was 37.12º in flexion and 32.93º in extension. The combined mean global range of motion was 70.05º for the HWL protocol. The flexion and extension flexibility curves demonstrated regions of increased stiffness as expected with viscoelastic tissue. Sample flexibility curves typical for the HWL protocol are show in **Figure 4.5**.

The HWL MSU percent contribution to global motion indicated significant differences from the PM and EL protocols as shown in **Figure 4.6**. In flexion, the HWL protocol significantly differed from the PM protocol at the C6-C7 and C7-T1 levels and

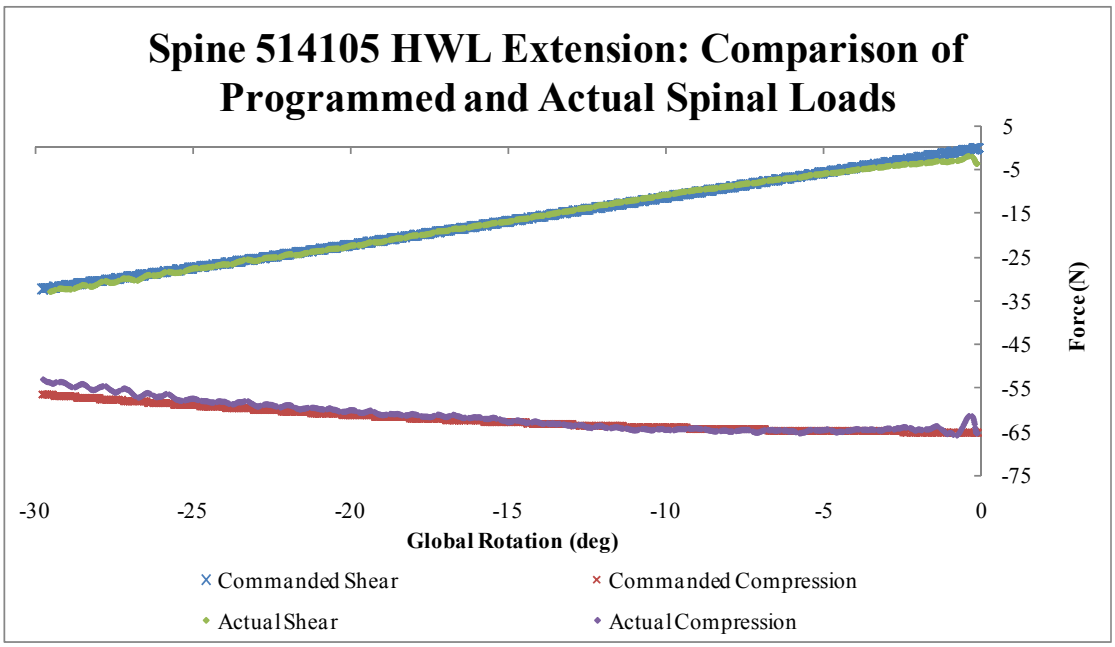

Figure 4.3. Sample extension commanded forces and actual applied forces

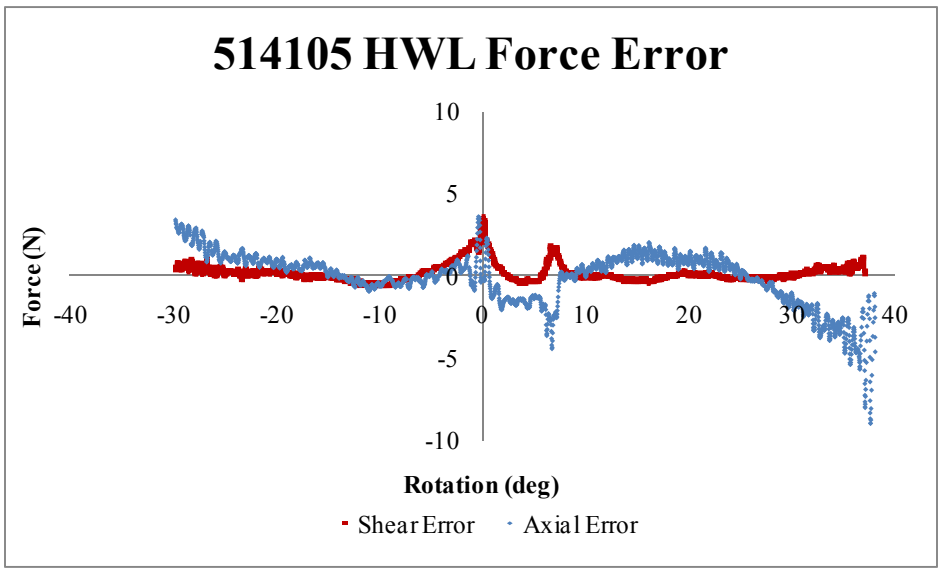

Figure 4.4. Sample force error curves in flexion and extension

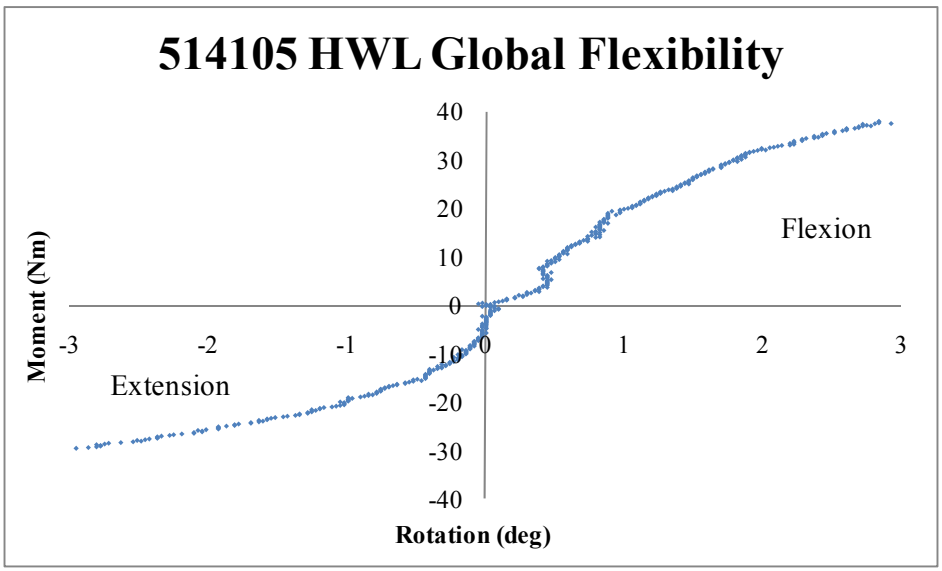

Figure 4.5. Sample flexion and extension global flexibility curves for the head weight loading protocol

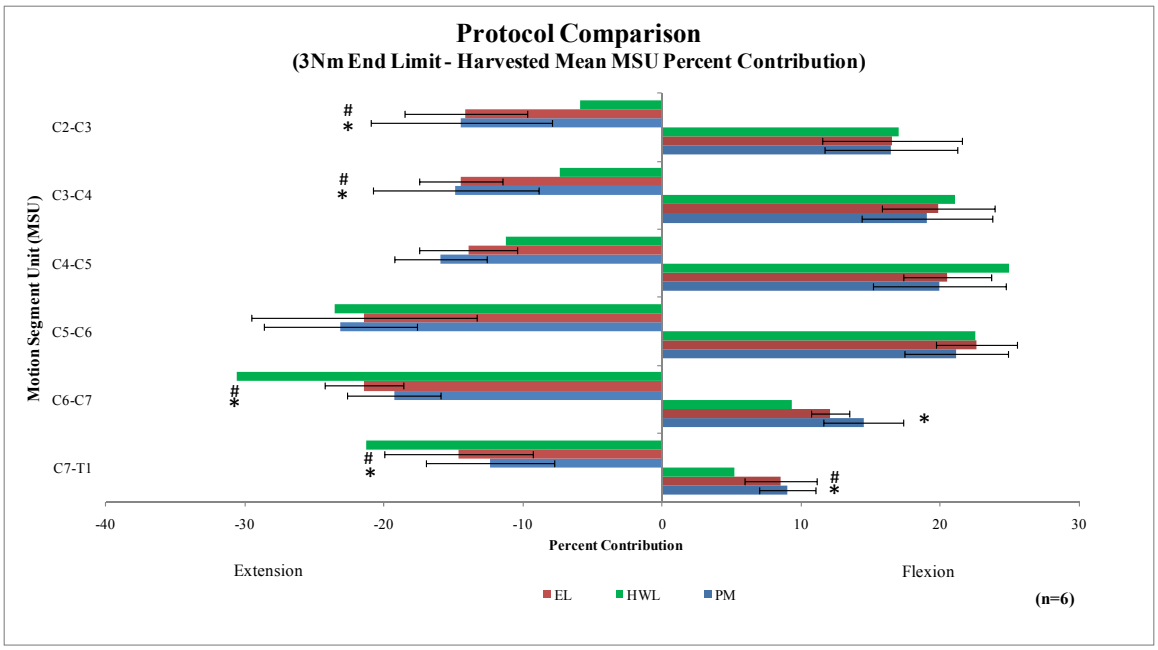

Figure 4.6. Segmental percent contribution relative to global motion in independent flexion and extension

from the EL protocol at C7-T1. In extension, the HWL protocol differed from both the EL and PM protocols at the C2-C3, C3-C4, C6-C7, and C7-T1 MSUs. The HWL protocol produced less motion at the lower levels in flexion, whereas in extension, the lower levels had much more motion compared to the other protocols while the upper levels had less.

The combined flexion and extension MSU percent contribution to global motion showed a significant difference between the HWL protocol and the EL and PM simulations at C2-C3. All other levels were not significantly different. **Figure 4.7** shows the overall shape of the combined motion response for all 3 protocols. The HWL protocol is similar to the EL and PM protocols with C5-C6 demonstrating the most motion. Furthermore, the independent flexion and extension ROM and the combined flexion and extension ROM did not produce significant differences between any of the simulated protocols.

4.3.4 Segmental Recruitment

Figure 4.8 shows a sample group of curves depicting the involvement of each MSU throughout the duration of a flexion or extension bend. The end limit trends in **Figure 4.6** are corroborated, but the PM and HWL protocols seem to recruit the segments at very different rates. The biggest contrast is at the C5-C6 level. The PM protocol recruits the MSU linearly, but the HWL protocol recruits the level quickly and essentially stops contributing to global motion after only 25% of the test. The caudal levels also show changes with the HWL protocol. The MSUs are recruited at the same rate as the PM protocol until a defined point where they suddenly get recruited faster. Finally, at the cranial levels, the HWL protocol has little to no contribution to global rotation in extension. In flexion, the levels are recruited toward the end limit of testing to levels similar to the PM protocol.

4.4 Discussion

4.4.1 Load Verification

The force control algorithm had more difficulty controlling the higher end loads in the HWL protocol than in the PM or EL protocols. The larger demand placed on the system had higher force errors and in some tests, regions of instability. **Figure 4.3** shows oscillations at the end of the flexion test. A recommendation was made to investigate a different gain setting function that would dampen the system response near the moment end limit to prevent oscillation. Despite the increased force error as compared to our experience with other testing protocols in the Spine Robot, the terminal error values at evaluated end load limits were on average within the ± 5 N target for flexion and within 25% of the ± 5 N target during extension.

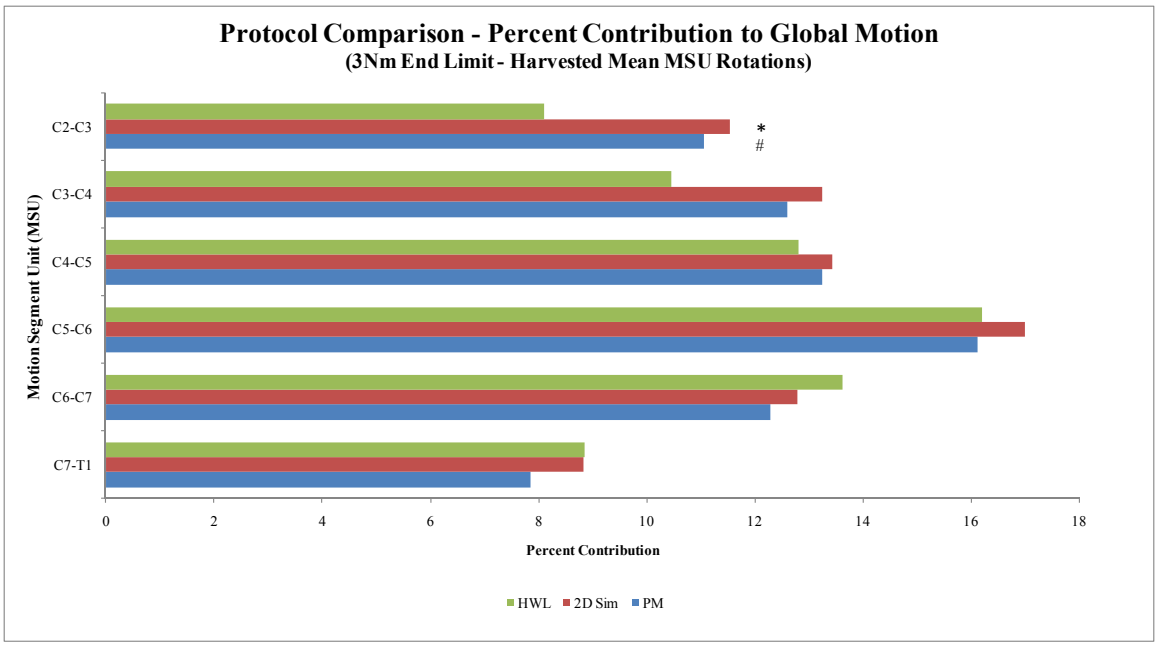

Figure 4.7. Simulated biomechanical testing protocols combined percent contribution to global rotation

Simulated head weight loading, eccentric loading, and pure moment protocols combined flexion and extension mean segmental percent contribution to global rotation. Significant differences were found between the head weight loading protocol and both the eccentric loading and pure moment protocols at the C2-C3 level. Differences are indicated by "#" and "*".

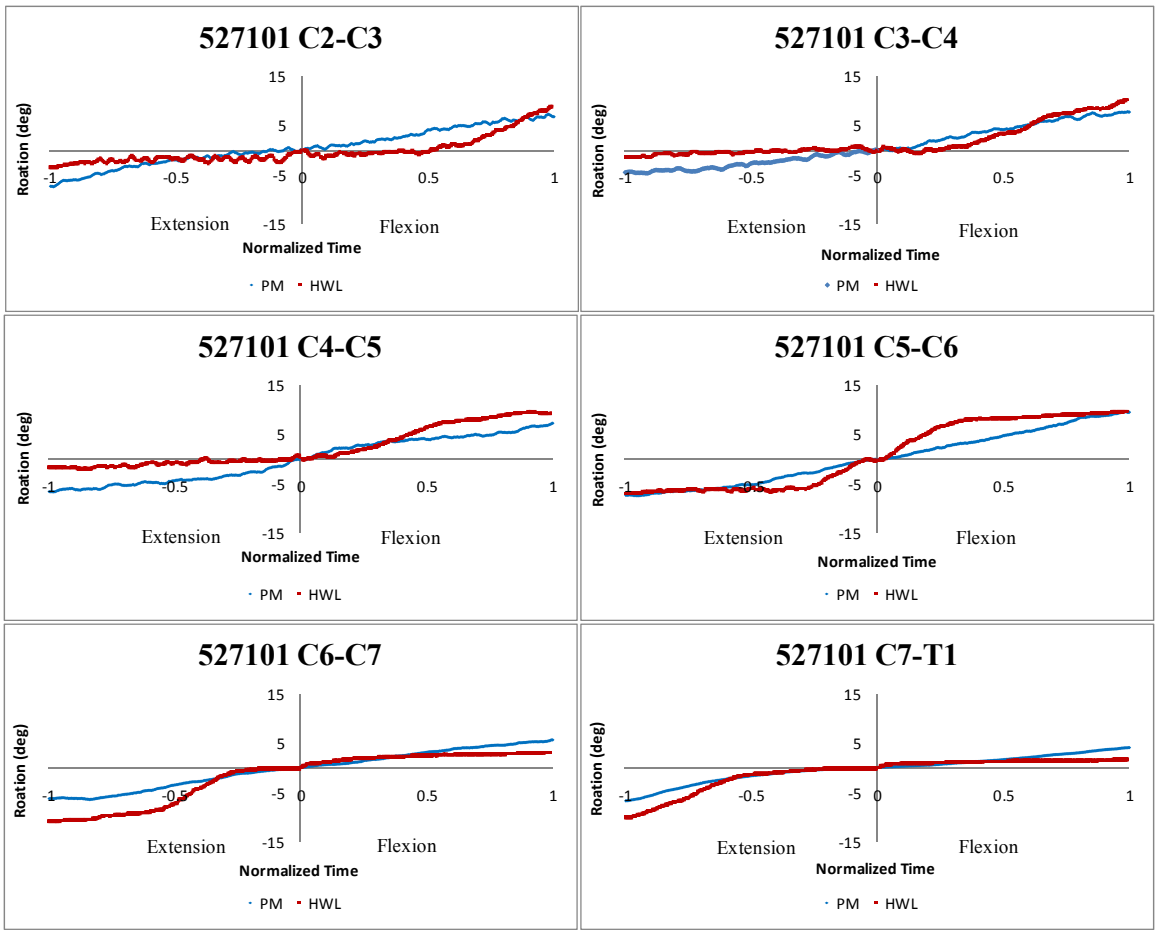

Figure 4.8. Sample head weight loading and pure moment flexion and extension segmental recruitment

Absolute motion segment unit rotation plotted versus a normalized time scale for flexion and extension for the simulated pure moment and head weight loading protocols.

4.4.2 Motion Response

In individual flexion and extension a significant trend is observed: the HWL protocol seems to drive a majority of the flexion rotation at the cranial four MSUs and drive extension with the caudal three MSUs. This is in stark contrast to the PM and EL protocols, where the MSUs exhibit a more gradual, centered (at C4-C5) bell curve motion profile. This result, however, is obscured when the rotations are combined. Six statistically different MSU contributions were reduced to one.

One limitation of the study is that the spine was not monitored during preloading. Patwardhan, 2000, has described a buckling effect of the cervical spine with loads higher than 10 N and lower than 40 N. The preload (and constant load) in this study was 65 N. However, the Patwardhan, 2000, study applied vertical loads to the free end of a spinal segment. The load application effectively created a bending moment and flexed or extended the spine depending on the location of the force vector. The spine robot applied a 65 N force to the rigidly fixed cranial end of the spinal specimen. The corresponding mean shear produced on the spine was 6.35 N. The relatively low level of shear force buildup with the compression suggests the spine was not over constrained in the antero-posterior direction. The mean moment offset was 2.13 Nm. This moment offset may have been the result of the vertical load being transferred anterior to the center of the caudal load cell due to specimen's alignment within the pots or anatomy. Since the spine was supported at both ends, application of the axial load may have induced bending resulting in a shift of MSU rotation to either flexion or extension. This rotational predisposition could be the cause of the different motion profile associated with the HWL protocol as well as the inherent moment offset.

Additionally, the isolation of the head weight as the main contributor to spinal forces might be an over simplification. There are numerous muscle forces present and in an optimal *in vitro* protocol, would need to be accounted for. Previous studies attempting to replicate neck muscle forces with complex fixtures and cable systems have demonstrated non physiologic sagittal motion profiles (Panjabi *et al*., 2001).

4.4.3 *In Vivo* Comparison

Numerous radiographical studies have been performed investigating cervical spine rotation. Often subjects are instructed how to move their head in the sagittal plane and maximal flexion and extension lateral radiographs are taken (Hsu *et al*., 2011; Penning *et al*., 1989; White *et al*., 1990). Many studies are only concerned with maximal range of motion and therefore do not take a baseline orientation. Without an image of the spine in its neutral orientation, it is impossible to separate flexion from extension. One study used a three image analysis (neutral, flexed, and extended) to study passive and active cervical spinal rotations. This study served as a good comparison for the HWL and PM protocols. The passive rotations were performed by a clinician while the subject was under anesthesia, whereas the active rotations were performed by the patients themselves. **Figure 4.9** shows the active and passive percent contribution to motion for the study

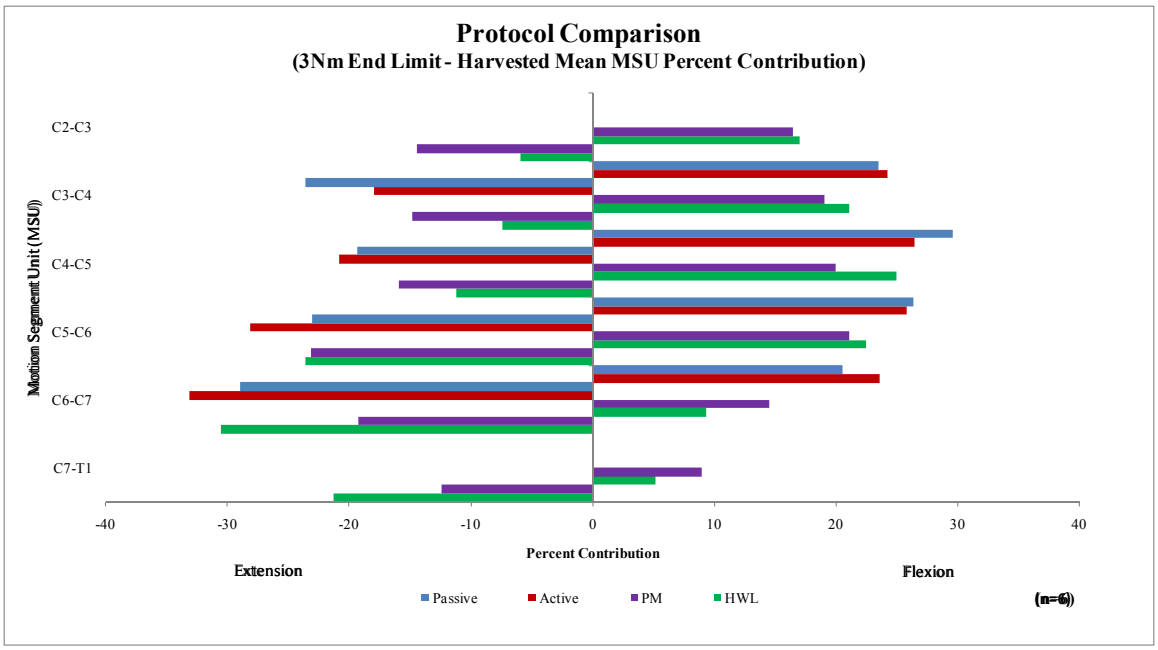

Figure 4.9. ***In vivo*** **active and passive motion responses compared with simulated protocol motion responses**

Mean active and passive in vivo motion segment unit percent contributions from Hsu, *et al,* 2011, compared to the simulated pure moment and head weight loading protocols. Percent contributions are separated into flexion and extension.

compared with the HWL protocol and previously simulated PM protocol. In flexion both the HWL and PM protocol follow general trends shown by the active and passive simulations. The most noticeable trend is in extension, where the *in vivo* study demonstrates a caudally increasing contribution of the MSUs in the active scenario. This is mirrored by the motion response of the HWL protocol. At the C6-C7 MSU, both *in vivo* contributions are at their greatest. The HWL protocol also has a peak contribution at C6-C7, whereas the PM peaks at C5-C6. Also of note, compared to their counterparts, the passive *in vivo* and the PM protocol, show a higher contribution in the cranial segments.

4.4.4 *In Vitro* Comparison

In addition to head weight, muscle forces are also involved in cervical spinal rotation. Some researchers have explored using a follower load to simulate the muscle forces (Miura *et al*., 2002; Panjabi *et al*., 2001; Patwardhan *et al*., 2000). Published rotation values for all subaxial cervical MSUs were difficult to find. Since no published work presented flexion and extension individually, combined rotation was used as a comparator. Miura published a paper utilizing a 100 N follower load augmenting a pure moment bending protocol to a 2 Nm moment end limit. The MSU motion response is shown with the HWL and simulated PM in **Figure 4.10**. The main detractor from the follower load dataset is the drop in rotation at the middle MSUs. This is not indicative of an *in vivo* motion response. Both the HWL and simulated PM protocols have the most rotation at the C5-C6 and C6-C7 MSUs. This is consistent with the numerous *in vivo* data sets, as is shown in **Figure 4.10**.

4.5 Conclusion

This study effectively demonstrated that different end loading conditions can produce significantly different segmental rotations. This shift may be in agreement with passive versus active motions seen during cervical extension in vivo. As such, it provided another approach to study the biomechanical response of the subaxial cervical spine. Due to a lack of descriptive *in vivo* data, it was not possible to conclude that the HWL protocol was an accurate *replication* of passive cervical spine motion. Compared to tradition biomechanical testing protocols utilizing cable applied pure moments and follower loads, the HWL better approximated the sagittal *in vivo* bending characteristics. It was the only protocol that has attempted to recreate and describe separate *in vivo* flexion and extension rotation. Additionally, it is the only protocol designed to maintain the constant vertical head weight force on the subaxial cervical spine. Future work with the HWL protocol will explore other modes of bending and spinal conditions.

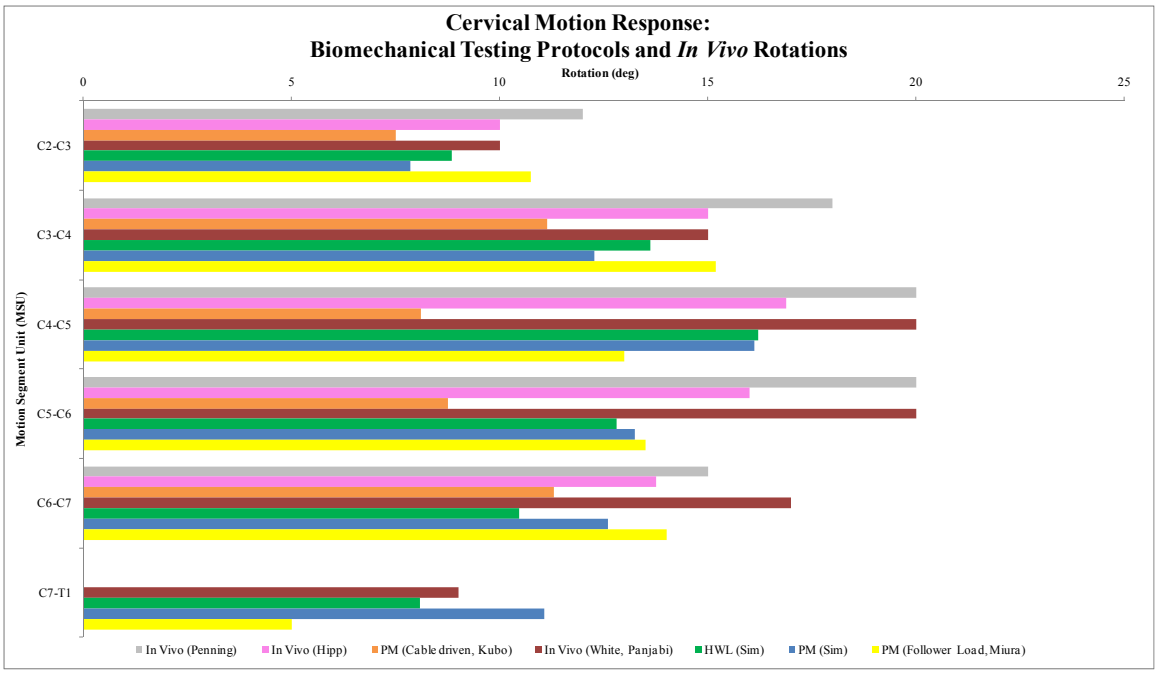

Figure 4.10. ***In vitro*** **and** ***in vivo*** **cervical motion response**

CHAPTER 5. LIMITATIONS AND CONCLUSIONS

The main limitations for this study are: 1) response of the force control algorithm, 2) capability of the hardware, 3) experimental scope, and 4) rigid mounting configuration. The first two limitations are related and defined by the robotic testing platform that was used. The scope of the study was limited to flexion and extension with a sample size of six. The spine robot fixtures were designed to secure each end of the spinal segment to the frame base and gimbal. Finally, no published *in vitro* studies delineate between flexion and extension rotations. The *in vivo* published data are similarly sparse. Though these limitations were present, the study was designed to maximize the potential of the spine robot and develop a unique loading protocol.

The Adept controller did not have an inherent force control feature. Furthermore, the positional control loops were inaccessible so they could not be modified to implement a force control routine. The only method for modulating a system response based on force was to create a software loop that manipulated the position. The potential for lag between the calculation, command output , and execution of the actual move could contribute to delays and instability resulting in non ideal force error buildup. Moving the force control algorithm inside the controller's control loop would enable much faster update rates and tighter force control.

The testing was limited to rotation in the sagittal plane. Full evaluation of the HWL protocol and its proximity to the *in vivo* motion response would require additional testing in lateral bending and axial rotation. Also, the study could be reinforced by adding specimen to the current sample consisting of six spines.

The Spine Robot has rigid fixation for the cranial and caudal specimen mounts. This is contrasted by traditional cable driven systems, because there is no "free end". Depending on the preload scenario, the spine could be supported in tension or compression. This setup therefore provides a degree of stability and it is unclear how this compares to stability provided to the spine by the ligaments and musculature in the *in vivo* scenario. Without the support, the spines could bend due to their inherent flexibility.

This study illustrated a limitation of the spinal biomechanics community as a whole. There is a lack of published literature describing segmental rotation in both *in vivo* and *in vitro* conditions. Often papers present data regarding one or two levels of interest instead of the entire cervical response. Of the papers that did detail entire cervical spinal motion, most of the rotations were combined flexion and extension profiles. This lack of information made it difficult to fully compare the simulated protocols to outside research. An attempt to present more descriptive data should be made by researchers in order to effectively cross compare results.

Two biomechanical testing protocols were programmed and simulated in a robotic based spine testing platform. The first emulated a gold standard pure moment bending protocol. The second was novel head weight loading protocol. Data for these protocols

for 6 sub-axial cervical spines was collected and compared against data for an existing simulated EL protocol. Control of targeted applied forces was reasonably well maintained within desired tolerances with suggestions for improvement provided above. When simulated on the Spine Robot, the MSU rotational responses between EL and PM protocols were not found to be different. This was surprising since traditional EL protocol motion profiles differed from published PM motion profiles. Further study should explore the efficacy of traditional PM test frames and the corresponding individual flexion and extension motion profiles. This study also demonstrated that large differences in end load conditions produce significantly different motion responses. However, those differing motion responses are only observed when flexion and extension are analyzed independently. Finally, the HWL protocol demonstrated motion trends similar to an *in vivo* study that presented flexion and extension separately. The Spine Robot demonstrated its ability to simulate standard biomechanical testing protocols and its adaptability to develop new protocols. The ability to create custom control algorithms for coordinated, multi-axis motion and high resolution position and force feedback make it a very powerful biomechanical test frame.

CHAPTER 6. RECOMMENDATIONS FOR FUTURE WORK

The first recommendation for future work would be to improve the force control algorithm. Currently, the program utilizes an “alter” command to modify the global spinal trajectory in each 4ms trajectory cycle. The path adjustment has a limited magnitude since it changes the location of proximal setpoints in the predefined trajectory path. Programming a “higher level” path modification could help resolve force errors faster. A path modification can be programmed in the “Continuous Path” loop based on the “alter” values combined with a force error offset. The force error offset would be calculated by the current force error and multiplied by a gain setting. The gain setting could be modified by the moment value to take into account specimen stiffness. The gain setting could also be adjusted based on force error trends, so as to recognize situations where the force error is drifting and possibly apply a stronger path correction.

More robust programming can also help improve the time needed to run the experiments. Currently, processing the data and generating new input trajectories at each iteration of spine testing takes the most time; more so than the test itself. An Excel macro or MatLab script could be written to automate the intermediate data processing. Eventually it would be desired to incorporate this automation into the V+ program so the entire test can be run without user involvement. Additionally, the program could be modified to run the final optimal path numerous times for cyclic testing and neutral zone investigations.

It would also be recommended that this study be expanded to alternate modes of bending. The cervical spine allows for head movement in all directions, so a future study incorporating lateral bending and axial rotation should be considered. Coupled bending scenarios should also be explored.

Finally, the novel HWL protocol should be employed for spinal instrumentation and surgical procedure studies. The protocol is unique in its ability to force additional extension rotation at the lower cervical levels. When used in conjunction with traditional biomechanical tests, the protocol has a more rigorous evaluation of the operated condition.

LIST OF REFERENCES

Alberts B, Bray D, Hopkin K, Johnson A, Lewis J, Raff M, Roberts K, Walter P. Essential cell biology. 2nd ed. New York: Garland Science; 2004.

Bonin H. *In-vitro analysis of the instantaneous center of rotation in a human cervical spine model using a spine robot* [thesis]. Memphis (TN): University of Tennessee Health Science Center; 2006.

CEEssentials.net [Internet]. Arvada,CO: TheNewPush, LLC; c2004-2011 [updated 2006 Aug; cited 2011 Mar 10]. Available from: http://www.ceessentials.net/article22.html.

Cervical-spine.org [Internet]. Denmark: Whiplash Connection; c2008-2011 [updated 2010 Sep 20; cited 2011 Mar 10]. Available from: http://www.cervical-spine.org/index.php/Overview:_Head-neck-joint_instabilities.

Chung S, Khan S, Diwan A. *The molecular basis of intervertebral disk degeneration*. Orthopedic Clinics of North America, 2003. **34**:200-219.

DiAngelo D, Foley K. *An improved biomechanical testing protocol for evaluation of a multilevel cervical instrumentation in a human cadaveric corpectomy model*. Spinal Implants: Are We Evaluating Them Properly? [ASTM Special Technical Publication], 2003. 155-172.

DiAngelo D, Robertson J, Metcalf N, et al. *Biomechanical testing of an artificial cervical joint and an anterior cervical plate*. Journal of Spinal Disorder Technology, 2003. **16**:314-323.

DiAngelo D, Scifert J, Kitchel S, et al. *Bioabsorbable anterior lumbar plate fixation in conjunction with cage-assisted anterior interbody fusion*. Journal of Neurosurgery, 2002. **4**:447-455.

Eguzabal J, Tufaga M, Sheer J, Ames C, Lotz J, Buckley J. *Pure moment testing for spinal biomechanics applications: fixed versus sliding ring cable-driven test designs*. Journal of Biomechanics, 2010. **43**:1422-1425.

Frasur K. *A passive pure moment protocol for testing spine segments: development and application* [thesis]. Memphis (TN): University of Tennessee Health Science Center; 2010.

Gay R, Ilharreborde B, Zhao K, Boumediene E, An K. *The effect of loading rate and degeneration on neutral region motion in human cadaveric lumbar motion segments*. Clinical Biomechanics, 2008. **23**:1-7.

Gilbertson L, Doehring T, Kang J. *New methods to study lumbar spine biomechancics: delinieation of in vitro load-displacement characteristics by using a robotic/UFS testing system with hybrid control*. Operative Techniques in Orthodpedics, 2000. **10**:246-253.

Goel V, Panjabi M, Patwardhan A, Doori, A, Serhan H. *Test protocols for evaluation of spinal implants*. Journal of Bone and Joint Surgery, 2006. **88**:103-109.

Goertzen D, Kawchuk G. *A novel application of velocity-based force control for use in robotic biomechanical testing*. Journal of Biomechanics, 2009. **42**:366-369.

Goertzen D, Lane C, Oxland T. *Neutral zone and range of motion in the spine are greater with stepwise loading than with a continuous loading protocol. An in vitro porcine investigation*. Journal of Biomechanics, 2004. **37**:257-261.

Gorinevsky D, Formalsky A, Schneider A. Force control of robotic systems. 1st ed. New York: CRC Press; 2001.

Hamill J, Knutzen K. Biomechanical basis of human movement. 2nd ed. New York: Lippincott Williams and Wilkins; 2003.

Hochman M, Tuli S. *Cervical spondylotic myelopathy: a review*. Internet Journal of Neurology [Internet]. 2009 Feb [cited 2011 Mar 10];4(1): [about 10 p.] Available from: http://www.ispub.com/ostia/index.php?xmlFilePath=journals/ijn/vol4n1/cervical.xml.

Hsu W, Chen Y, Lui T, Chen T, Hsu Y, Lin C, Tsai M. *Comparison of the kinematic features between the in vivo active and passive flexion-extension of the subaxial cervical spine and their biomechanical implications*. Spine. [ahead of print].

Kelly B. *A multiaxis programmable spine robot for the study of multibody spinal biomechanics using real-time hybrid force and displacement control strategies* [dissertation]. Memphis (TN): University of Tennessee Health Science Center; 2005.

Kelly B. (2011) *Eccentric loading protocol simulation in a programmable spine robot*. Unpublished manuscript.

Kim D, Cammisa F, Fessler R, editors. Dynamic reconstruction of the spine. 1st ed. New York: Theime Medical Publishers; 2006.

Kubo S, Goel V, Yang S, Tajima N. *Biomechanical evaluation of cervical double door laminoplasty using hydroxyapatite spacer*. Spine, 2003. **28**:227-234.

Lysack J, Dickey J, Dumas G, Yen D. *A continuous pure moment loading apparatus for biomechanical testing of multi-segment spine specimens*. Journal of Biomechanics, 2000. **33**:765-770.

Mcinerney J., Ball P. The pathophysiology of thoracic disc disease. Neurosurgical Focus [Internet]. 2000;9(4): [about 5 p.] Available from: http://www.medscape.com/viewarticle/405642_1.

Miura T, Panjabi M, Cripton P. *A method to simulate in vivo cervical spine kinematics using in vitro compressive preload*. Spine, 2002. **27**:43-48.

Nordin M, Frankel V, editors. Basic biomechanics of the musculoskeletal system. 3rd ed. New York: Lippincott Williams and Wilkins; 2001.

Panjabi M. *Hybrid multidirectional test method to evaluate spinal adjacent-level effects.* Clinical Biomechanics, 2007. **22**:257-256.

Panjabi M, Miura T, Cripton P, Wang J, Nain A, DuBois C. *Development of a system for in vitro neck muscle force replication in whole spine experiments*. Spine, 2001. **26**:2214-2219.

Patwardhan A, Havey R, Meade K, et al. *A follower load increases the load-carrying capacity of the lumbar spine in compression*. Spine, 1999. **24**:1003-1009.

Patwardhan A, Havey R, Meade K, et al. *The load-carrying capacity of the human cervical spine is increased under a follower load*. Spine, 2000. **25**:1548-1554.

Penning L. *Normal movements of the cervical spine*. American Journal of Roentgenology, 1978. **130**:317-236.

Puttlitz C, Rousseau M, Xu Z, Hu S, Tay B, Lotz J. *Intervertebral disc replacement maintains cervical spine kinetics*. Spine, 2004. **29**:2809-2814.

Reitman C, Mauro K, Nguyen L, Ziegler J, Hipp J. *Intervertebral motion between flexion and extension in asymptomatic individuals*. Spine, 2004. **24**:2832-2843.

Siddharthan K, Nelson A. *A business case for patient care ergonomic interventions*. Nursing Administration Quarterly, 2005. **29**:63-71.

Urban J, Roberts S, Ralphs J. *The nucleus of the intervertebral disc from development to degeneration*. American Zoology, 2000. **40**:53–61.

Vallfors B. *Acute, subacute and chronic low back pain: clinical symptoms, absenteeism and working environment*. Scandinavian Journal of Rehabilitation Medicine, 1985. **11**:1-98.

Walker M, Dickey J. *New methodology for multi-dimensional spinal joint testing with a parallel robot*. Medical Bio Engineering Computing. 2007. **45**:297-304.

White A, Panjabi M. Clinical biomechanics of the spine. 2nd ed. Philadelphia: J.B. Lippincott; 1990.

Wido D. (2011) *Use of a spine robot to simulate and compare a pure moment and eccentric loading protocol*. Unpublished manuscript.

Wilke H, Rohlmann A, Neller S, Schulteib M, Bergmann G, Graichen F, Claes L. *Is it possible to simulate physiologic loading conditions by applying pure moments? A comparison of in vivo and in vitro load components in an internal fixator*. Spine, 2001. **26**:636-642.

Zhao C, Wang L, Jiang L, Dai L *The cell biology of intervertebral disc aging and degeneration*. Ageing Research Reviews, 2007. **6**:247-261.

APPENDIX A. SPINE ROBOT

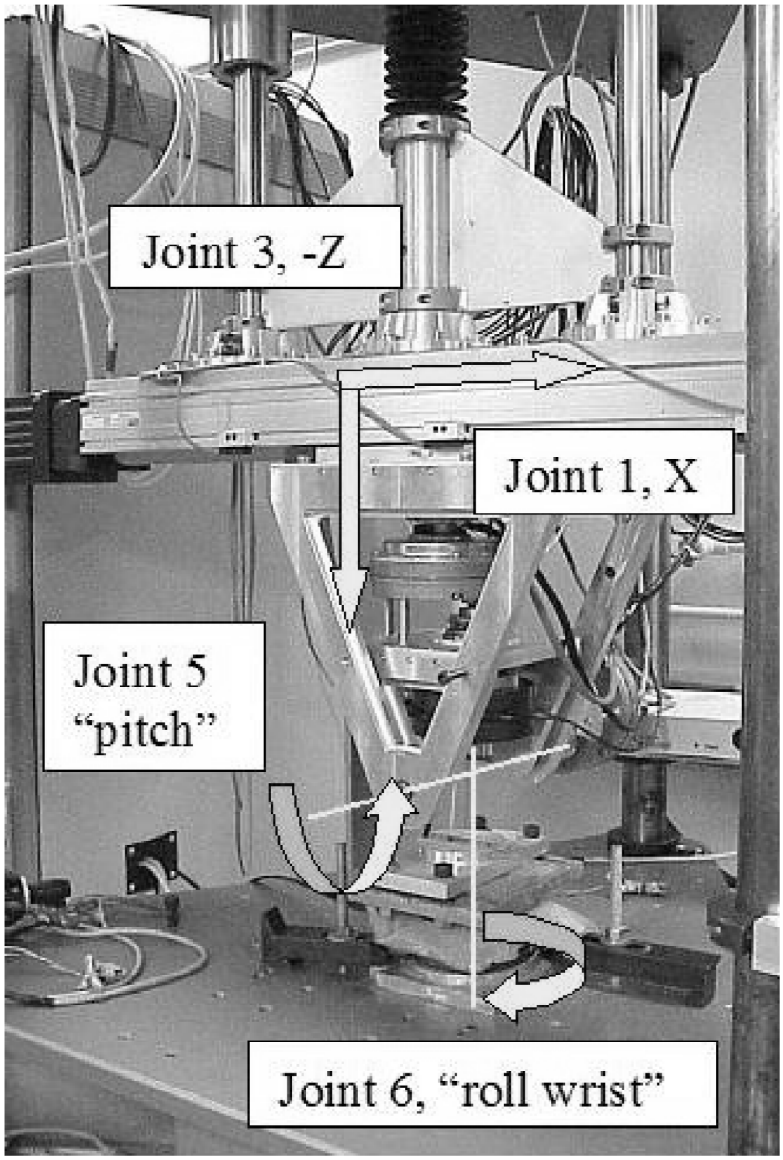

Figure A.1. Spine Robot with degrees of freedom labeled

Adapted with permission from Kelly B. *A multiaxis programmable spine robot for the study of multibody spinal biomechanics using real-time hybrid force and displacement control strategies* [dissertation]. Memphis (TN): University of Tennessee Health Science Center; 2005.

APPENDIX B. REAL TIME FORCE CONTROL CODE: INPUT AND FLEXION

```
GLOBAL REAL f[], start[], exit[], tcp[,], coef[,], wcor[,], pos[,], fs[,], ferror[,], t[]
?       GLOBAL REAL fg[], x[], p[,], f[,]
?       GLOBAL REAL axr, bxr, azr, bzr, rule, combined.flag1, combined.flag2, speedset, accelval, accelper, axrot, pzrotgain
?       GLOBAL REAL rot, srot, zdist, shearerr, cosax, sinax, sinpitch, cospitch, dx, dz, sign, tor.looptotal, axf, bxf
?       GLOBAL REAL azf, bzf, theta, thetamax, m1, m2, mz, pxstartgain, pzstartgain, rule.flag1, rule.flag2, delmsag, fz
?       GLOBAL REAL looptotal, axe, bxe, aze, bze, pxgain, pzgain, startrot, exitrot
?       GLOBAL REAL preload_value
?       GLOBAL LOC start1.loc, test.start.loc, start.loc, exit.loc, tor.loc[], loc[]
?       GLOBAL $ans, $ans1, $ans2, $menu
?       GLOBAL $specimen_name
?       GLOBAL REAL iteration
?       GLOBAL $rot_string
?       GLOBAL $iter_string

        $specimen_name = "null"
        iteration = 1

        preload_value = -10
        x[5] = 0
        f[5] = 0
        fg[5] = 0
        start[5] = 0
        exit[5] = 0
        tcp[4,100] = 0
        coef[4,100] = 0
        p[6,900] = 0
        f[6,900] = 0
        wcor[1,10000] = 0
        pos[3,10000] = 0
        fs[7,10000] = 0
        ferror[1,10000] = 0
        t[10000] = 0
        SET tor.loc[7500] = TRANS(0,0,0,180,180,0)
        SET loc[10000] = TRANS(0,0,0,180,180,0)

        ai.version = 1302
?       SPEED 100 MONITOR
?       ENABLE SCALE.ACCEL
?       CPON

?       SELECT FORCE = 1
?       FORCE.MODE (21)
?       FORCE.FRAME (1) TRANS(,,-51.549)
?       FORCE.MODE (10) 4.45
?       FORCE.MODE (11) 0.0254
?       FORCE.MODE (12) 5        ;this value will influence output, 5 is best
?       FORCE.MODE (13) 3
?       FORCE.MODE (14) 6
?       FORCE.OFFSET (0)
?       FORCE.MODE (1) ^H21, 50   ;Master guard mode in z-x plane

?       SELECT FORCE = 2
?       FORCE.MODE (21)
?       FORCE.MODE (10) 4.45
?       FORCE.MODE (11) 0.0254
?       FORCE.MODE (12) 5        ;this value will influence output, 5 is best
?       FORCE.MODE (13) 3
?       FORCE.MODE (14) 6
?       FORCE.OFFSET (0)

    5  combined.flag1 = 0
       combined.flag2 = 0
       TYPE /C50, /U40
       TYPE " "
```

```
    TYPE "      ************************************************************"
    TYPE "                        MAIN SELECTION MENU                       "
    TYPE "      ************************************************************"
    TYPE " "
    TYPE "          Testing Protocol                Numeric Selection     "
    TYPE "         ------------------------------------------------------------"
    TYPE " "
    TYPE "          Mount a test specimen ..... 1"
    TYPE " "
    TYPE "          Perform a pure torsion test ..... 2"
    TYPE " "
    TYPE "          Perform a pure flexion test (ok)..... 3"
    TYPE " "
    TYPE "          Perform a pure extension test ..... 4"
    TYPE " "
    TYPE "          Perform combined torsion + flexion test ..... 5"
    TYPE " "
    TYPE "          Perform combined torsion + extension test ..... 6"
    TYPE " "
    TYPE "          Turn off high power; safely work in robot space .. 7"
    TYPE " "
    TYPE "          Exit to system monitor ..... 8"
    TYPE " "
    PROMPT "          Please enter a selection: ", $menu

    IF ($menu <> "1") AND ($menu <> "2") AND ($menu <> "3") AND ($menu <> "4") AND ($menu <> "5") AND ($menu <>
"6") AND ($menu <> "7") THEN
       IF $menu <> "8" GOTO 5
    END ;if

    CASE TRUE OF
      VALUE $menu == "1":
        PROMPT "How much compression on spine would you like? (neg value)", compression_val
        preload_value = compression_val+10
        CALL spine.mount()
      VALUE $menu == "2":
        GOTO 1000
      VALUE $menu == "3":
        GOTO 2000
      VALUE $menu == "4":
        GOTO 3000
      VALUE $menu == "5":
        combined.flag1 = 1
        GOTO 1000
      VALUE $menu == "6":
        combined.flag2 = 1
        GOTO 1000
      VALUE $menu == "7":
        GOTO 10
      VALUE $menu == "8":
        GOTO 20
    END
    GOTO 5

  10  DETACH (0)
    TYPE /C2, "Turn off high power, then perform work within robot space. "
    PROMPT " When ready restore high power and press 'y' ", $ans
    IF $ans <> "y" GOTO 10
    IF STATE(1) == 2 THEN
       TYPE " "
       TYPE " You have not restored robot high power!!"
       GOTO 10
    END
    ATTACH (0)
    GOTO 5

  20  TYPE " "
    PROMPT "Are you sure you wish to exit? (y/n)", $ans2
    IF ($ans2 <> "y") AND ($ans2 <> "n") THEN
       GOTO 20
```

VITA

Daniel Mark Wido was born in 1985 to Mark and Judy Wido in Belleville, IL. He has a younger sister named Katherine. After graduating from high school in Naperville, IL, he attended college at the Illinois Institute of Technology where he majored in Biomedical Engineering with a minor in Biochemistry. Daniel pursued his Master of Science in Biomedical Engineering at the University of Tennesee Health Science Center, with a research focus on *in vitro* spinal biomechanical testing protocols.